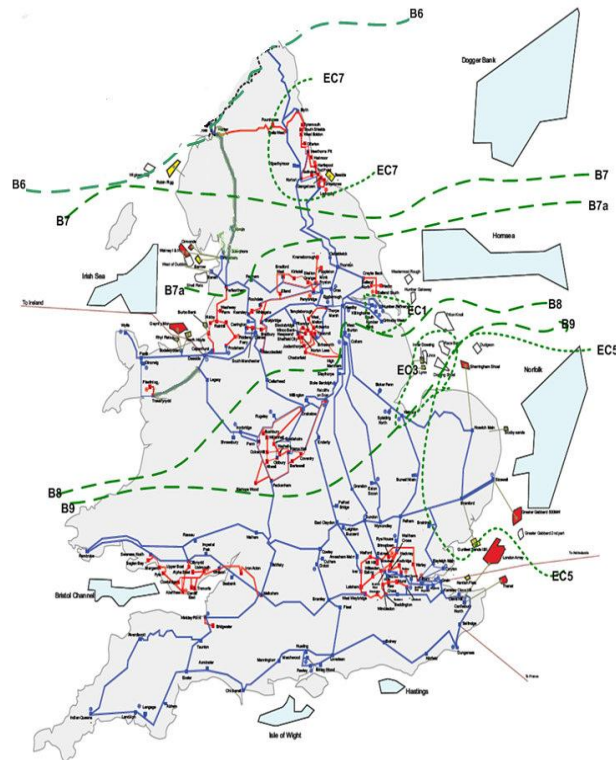


Journal of Energy Challenges and Mechanics

ISSN 2056-9386

<http://www.nscj.co.uk/JECM/>

Volume 2, Issue 1
January 2015



Featured article:

Integrated Offshore Transmission

Dr. Biljana Stojkovska, Faith Natukunda, Sheriff Ilesanmi*

National Grid, Warwick, CV34 6DA, UK

Journal of Energy Challenges and Mechanics, volume 2, pages 15-22.



North Sea Conference & Journal LTD
2 Charlestown Walk, Cove Bay, AB12 3EZ, Aberdeen, Scotland, United Kingdom
<http://www.nscj.co.uk/JECM/> | jecm@nscj.co.uk | +44(0)1224 875635



TABLE OF CONTENTS

pages

ECM Series Interview: Prof. Chadwick Dearing Oliver, School of Forestry and Environmental Studies, Yale University – Dr. Henry Tan, University of Aberdeen ([video](#))

[Article 1](#): Stress-dependent permeability of two-solid constituent model of gas shales 1-5

*Mikhail B. Geilikman**, *Sau-Wai Wong*, *John M. Karanikas*
Shell International Exploration and Production Inc., Houston, TX 77251, USA

[Article 2](#): Reliability analysis of complex limit states of floating wind turbines 6-9

*Athanasios Kolios**, *Michael Borg*, *Dawid Hanak*
Division of Energy and Power Engineering, School of Engineering, Cranfield University, UK

[Article 3](#): Fleet Monitoring for Distributed Energy Systems 10-14

*Marc Hilbert**, *Tobias Vraetz*, *Andrea Kulanthavadi*, *Karl Nienhaus*
Institute for Mining and Metallurgical Machinery, RWTH Aachen University, Aachen, Germany

[Article 4](#): Integrated Offshore Transmission 15-22

*Dr. Biljana Stojkovska**, *Faith Natukunda*, *Sheriff Ilesanmi*
National Grid, Warwick, CV34 6DA, UK

[Article 5](#): A new configuration of vertical axis wind turbine: an overview on efficiency and dynamic behaviour 23-28

Mario R. Chiarelli¹, *Andrea Massai²*, *Davide Atzeni^{1*}* and *Francesco Bianco¹*
¹*Department of Civil and Industrial Engineering, University of Pisa, Pisa, Italy*
AM Engineering, Firenze, Italy



Stress-dependent permeability of two-solid constituent model of gas shales

页岩气两固体成分模型的应力相关渗透率

Mikhail B. Geilikman*, Sau-Wai Wong, John M. Karanikas

Shell International Exploration and Production Inc., Houston, TX 77251, USA

mikhail.geilikman@shell.com

Accepted for publication on 23rd December 2014

Abstract - Because gas shales consist of organic and inorganic solid components, the stress and pore pressure dependence of permeability of shale gas rock is considered in the model of porous medium with two solid constituents. It is done in the framework of a generalized model of composite sphere phases each of them being gas/fluid saturated. It is shown that the total mean stress in each of the phases is different from the confining stress even for a homogeneous state. This leads to a more complicated dependence of permeability rather than that of Terzaghi effective stress, i.e. confining stress minus pore pressure as in the case of a one-solid constituent porous medium. Additional dependence of permeability on pore pressure is captured by considering Knudsen and slip flow contributions. Because depletion-induced variation of pore pressure leads to the variation of eigen-strain, the resultant strain and stress exerted at the reservoir by surrounding country rock is found by using Eshelby-type inclusion model. The depletion-induced evolution of reservoir permeability is expressed as a function of pore pressure. The model provides recommendation for maximum drawdown which still allows preventing collapse of porosity and permeability of softer organic constituent.

Keywords – gas shales, effective stress, permeability

I. INTRODUCTION

Due to the fact the shale gas rock is constituted by at least two main solid components with sufficiently different mechanic properties: organic matter and inorganic one, we would like to consider how this feature affects dependence of effective medium permeability on stress and pore pressure. As usual we assume [1] that permeability, k , is some function of porosity, ϕ : $k(\phi)$. In conventional theory of poro-elasticity variation of porosity is a function of Terzaghi effective stress [2]:

$$\Delta\phi = (\alpha - \phi_0) \cdot \frac{\Delta p - \Delta\sigma_v}{K_b} \quad (1)$$

where p is pore pressure, α is Biot's constant, $\Delta\sigma_v$ is increment of total mean stress (positive in compression), ϕ_0 is initial porosity, and K_b is drained bulk modulus of porous medium. The average stress, $\Delta\sigma_v$, in the eq. 1 relates to the stress in the part of rock, the porosity is defined for. If the rock has only one solid porous constituent, then the average stress is unique. Situation might be different if there are two or more solid constituents in porous medium. The local variations of stress in the different solid components are the same as global one only in some special cases [3]. Stress dependence of permeability is particularly important for the case of low porosity because stress increase may effectively close some flow paths. In that sense the system is close to percolation threshold. Due to small pore size, which is comparable with the mean free path of molecular motion, matrix permeability should also include Knudsen and slip flow components as well as conventional Poiseuille one [1]. It is important to know variation of reservoir permeability as a function of pressure as it changes as a result of depletion and compaction. It depends on interaction between reservoir and surrounding country-rock. For conventional reservoirs, it was described by Eshelby-type inclusion approach [4, 5] we would like to extend this approach to gas shale rock.

II. STRESS-DEPENDENT POROSITY IN PO-ROUS MEDIUM WITH TWO SOLID COMPONENTS

Gas shale rock has at least two solid constituents that are shale (with some carbonate content as well) and organic matter, i.e. kerogen. Unfortunately, at this point it is difficult to conclude from rock characterization data (SEM etc) which phase is continuous (connected) and which phase can be considered as an inclusion. The case when both phases (organic matter and shale) are continuous cannot be ruled out.

We generalize a simple model of composite material, specifically a “composite sphere model” (see [6] and reference therein) which was originally developed for non-porous composite media.

The structure of this generalized model can be described as a fractal one because the composite spherical arrangements of two phases of different gradation are assembled in the filling configuration while having the same proportion of two phases in them (denoted “*m*” and “*i*”) as it is shown at the Fig. 1. Each phase is a porous material with its own porosity and mechanical properties. In our model both phases, *m* and *i*, are saturated with pore fluid. The inner sphere is constituted by porous phase “*i*” with radius denoted as *a*.

The phase “*m*” fills the space between the boundary of inner sphere and the boundary of outer sphere, denoted as *b*. It is assumed that distribution of composite spheres with respect to their total radius *b* is random but in each sphere the ratio of *a/b* is the same. This means that volumetric fraction of phase “*i*” in the whole rock is equal to $c = (a/b)^3$. We consider that mechanical properties are different in *m* and *i* phases including Biot’s coefficients. It should be noted that we consider here a homogenous state of equilibrium, so the pore pressure is constant and is the same in both phases.

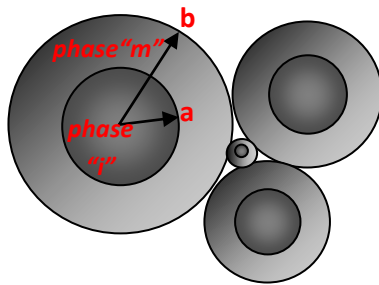


Figure 1. Composite porous sphere 3D model (schematic)

Using results of this model we can find stress in all constituents separately. For the sake of brevity we omit intermediate calculation and give formulas for mean total stress in both phases. A more detail formulation of the model is described in a separate publication [7].

Average total stress in *m*-phase

$$\sigma_{m,v} = \frac{p_c}{1+c} - \frac{p}{1+c} \left[\alpha_m + c \frac{4G_m (\alpha_i - \alpha_m)}{3K_i + 4G_m} \right] + \alpha_m p \quad (2)$$

and mean total stress in phase *i*:

$$\sigma_{i,v} = p_c \frac{1+f}{1+c} - \frac{p}{1+c} \left[\alpha_m + \frac{(3K_m + 4G_m) c (\alpha_i - \alpha_m)}{3K_m + 4G_m} \right] + \alpha_i p \quad (3)$$

where coefficient

$$f \equiv \frac{4G_m (K_i - K_m)}{K_m (3K_i + 4G_m)} \quad (4)$$

p_c is confining stress, p is pore pressure, c is volume fraction of *i* phase, K and G are drained bulk and shear moduli respectively, and α_i, α_m are Biot’s coefficients in *i* and *m* phases respectively. The stresses in *i*- and *m*- phases are shown at Figures 2 and 3.

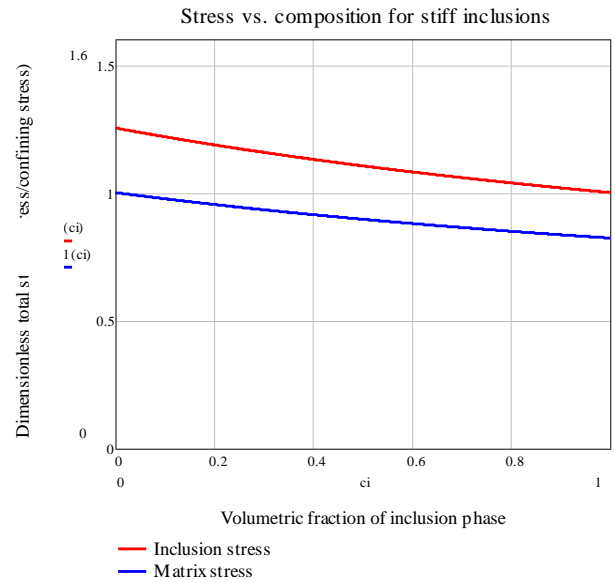


Figure 2. Total dimensionless stresses for matrix, $\sigma_{m,v}/p_c$ and inclusion, $\sigma_{i,v}/p_c$ vs. composition c in inclusion and matrix phases when inclusion is stiffer than matrix: $K_i=3K_m$.

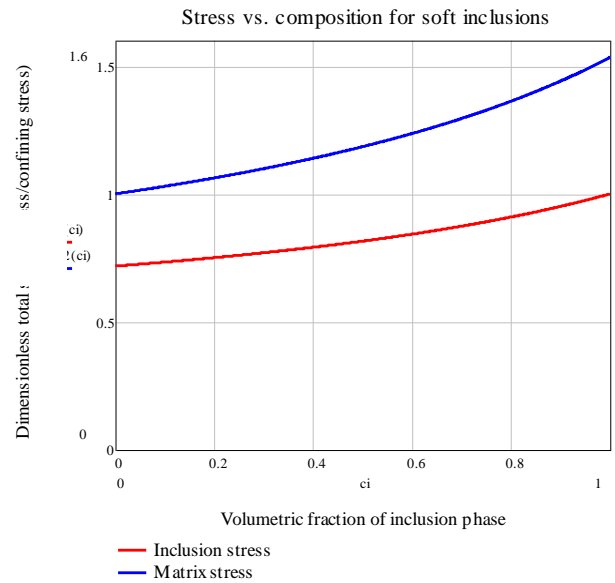


Figure 3. Total dimensionless stresses for matrix $\sigma_{m,v}/p_c$, and inclusion, $\sigma_{i,v}/p_c$, vs. composition c in inclusion and matrix phases when inclusion is softer than matrix: $K_i=K_m/3$.

The average stress in the rock is calculated as follows:

$$\sigma_v = c \sigma_i + (1 - c) \sigma_m \quad (5)$$

and after substitution of eqs. (2) and (3) into (5), we obtain for total average stress:

$$\sigma_v = p_c \quad (6)$$

as it should be under exerted confining stress p_c . For effective average stress we obtain from:

$$\sigma'_v = p_c - \alpha p \quad (7)$$

and effective Biot's coefficient for two-solid-component porous medium reads:

$$\alpha = \frac{c\alpha_i(3K_m + 4G_m) + (1-c)\alpha_m(3K_i + 4G_m)}{c(3K_m + 4G_m) + (1-c)(3K_i + 4G_m)} \quad (8)$$

The expression for porosity (1) is valid for each porous phase separately, if using the mean stress for the given phase. After substitution of the expression for mean stress eq. (2) and (3) in the eq.(1) we obtain for stress dependent porosity:

$$\phi_m = \phi_{0m} - (\alpha_m - \phi_{0m}) \cdot \frac{\Delta p_c - \gamma_m \Delta p}{(1+c f) K_m} \quad (9)$$

where coefficient

$$\gamma_m = 1 + c f (1 - \alpha_m) + c \frac{4G_m(\alpha_i - \alpha_m)}{3K_i + 4G_m} \quad (10)$$

As we can see coefficient γ_m can be potentially higher than 1 if the phase m is softer than phase i . For a single solid constituent porous medium, when $c = 0$, coefficient γ_m is equal to unity as it should be in conventional theory of poroelasticity for one-solid component porous medium.

Similarly for the i -phase porosity is expressed as follows:

$$\Delta\phi_i = -(\alpha_i - \phi_{0i}) \cdot \frac{1+f}{(1+c f) K_i} (\Delta p_c - \gamma_i \Delta p) \quad (11)$$

where coefficient

$$\gamma_i = (1 - \alpha_i) \cdot \frac{1+c f}{1+f} + \alpha_m + \frac{(3K_m + 4G_m c)(\alpha_i - \alpha_m)}{3K_m + 4G_m} \quad (12)$$

Again when the phase “ i ” occupies the whole volume, so that for $c = 1$, the coefficient $\gamma_i = 1$ as in conventional theory of poroelasticity. Numerical behavior of the coefficients γ_i and γ_m are shown at Figures 4, 5.

It should be noted that our model should not be mixed up with Zoback-Byerlee model [8] which explored a stiff and soft materials arrangement around each pore, whereas we consider two macroscopic porous phases of different stiffness.

Different effective stress rule for porosity arises due to difference in mean stresses for the phases m and i from the average mean stress in the whole porous medium as it is shown at Figs. 2 and 3 for the cases of soft and stiff inclusions.

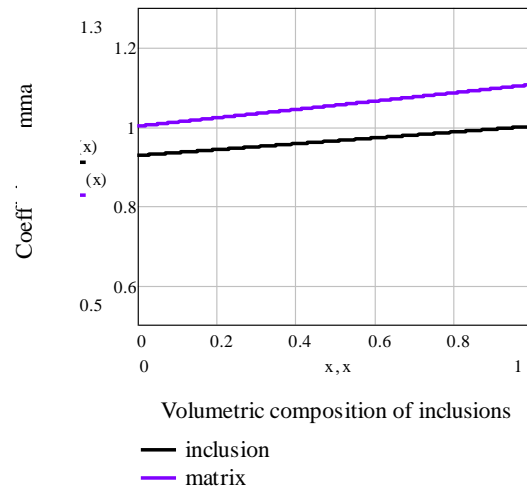


Figure 4. Pore pressure coefficients γ_i and γ_m given by eqs. (10) and (12) when inclusion is stiffer than matrix: $K_i = 3K_m$.

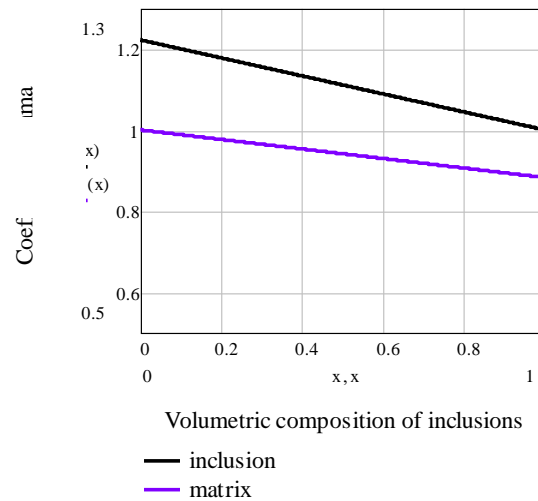


Figure 5. Pore pressure coefficients γ_i and γ_m given by eqs. (10) and (12) when inclusion is softer than matrix: $K_i = K_m / 3$.

The Biot effective stress rule for strain and Terzaghi effective stress rule for porosity still holds true but separately in each of the constituent phases.

As we can see from Figs. 2 and 3 our model gives correct crossover transition to the limit cases of one-component porous media of $c=0$ and $c=1$ when total stress must be equal to confining stress p_c (or in dimensionless units equal to 1).

III. PERMEABILITY OF COMPOSITE MEDIUM

There were numerous efforts in the past to derive effective properties of composite media. Effective permeability can be estimated approximately [6] as follows:

$$k_{eff} = k_m \left[1 + \frac{3c}{(1-c) + 3k_m / (k_i - k_m)} \right] \quad (13)$$

Because in general permeability is a function of porosity [1]: $k = k(\phi)$, after using explicit expression for porosity in inclusion and matrix (9), (11) we obtain that permeability of composite medium is a function of the following variables:

$$k_{eff} = k(p_c - \gamma_m p, p_c - \gamma_i p, p) \tag{14}$$

If permeability of i -phase (inclusion) is negligible, then from eq. (13) effective permeability:

$$k_{eff} \approx k_m \frac{2(1-c)}{2+c} \tag{15}$$

which means that effective permeability reads:

$$k_{eff} \approx k(p_c - \gamma_m p, p) \tag{16}$$

For non-adsorbing gas saturation, the separate dependence of permeability on pore pressure (the second variable in the eq. (16) is only due to Knudsen and slip flow. It means that for high pressure when these effects are not important, and the stress dependence of permeability reduces to one variable, $p_c - \gamma p$.

If experimental measurements of permeability of gas shales can be fitted better by some linear combination of confining stress and pore pressure: $p_c - \chi p$ with $\chi \neq 1$ [9, 10] it does not mean that Terzaghi effective stress rule for porosity is not valid but could be an indication that the rock contains several solid constituents with different elastic properties of the components. It is the case for gas shales where kerogen constituent is significantly softer (-3-4 times) compared to inorganic constituent (e.g. calcite).

Finding an adequate description of permeability in shale gas is a challenging problem because of complexity of the rock which contains both organic and non-organic components. It is also important to capture the following features of gas shale systems:

1. A model of Klinkenberg effect: due to small pore size, which is comparable with the mean free path of molecular motion, matrix permeability should include Knudsen and slip flow components as well as conventional Poiseuille one. In order to address this feature we have implemented Scott-Dullien model [11] as well as Ottani-Wakao-Smith model [12]. Both of the models are able to provide crossover from viscous Poiseuille flow in pores to Knudsen flow with molecular streaming for small pores.
2. Because gas methane can be adsorbed and desorbed by solid constituents (primarily by organic phase) the sorption-desorption induced strain and associated with it stress should be taken into account. We have implemented the open-system geomechanics approach as that in a system with variable solid mass (see [7] and references therein);
3. Estimation of reservoir permeability vs. pore pressure only based on the model results and Eshelby inclusion approach which allows to exclude stress.

These details can be found in our extended paper [7] and briefly presented at the Figs. 6 and 7.

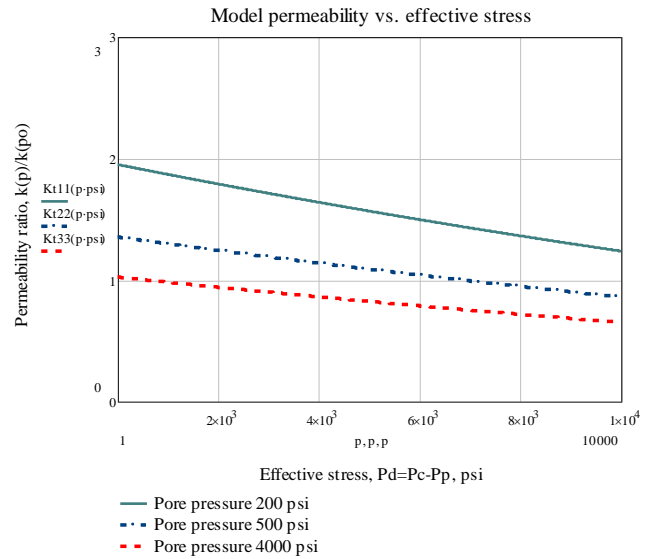


Figure 6. Model permeability as a function of pore pressure; effective Terzaghi stress, p_d , is equal to confining stress minus pore pressure: $p_d = p_c - p$.

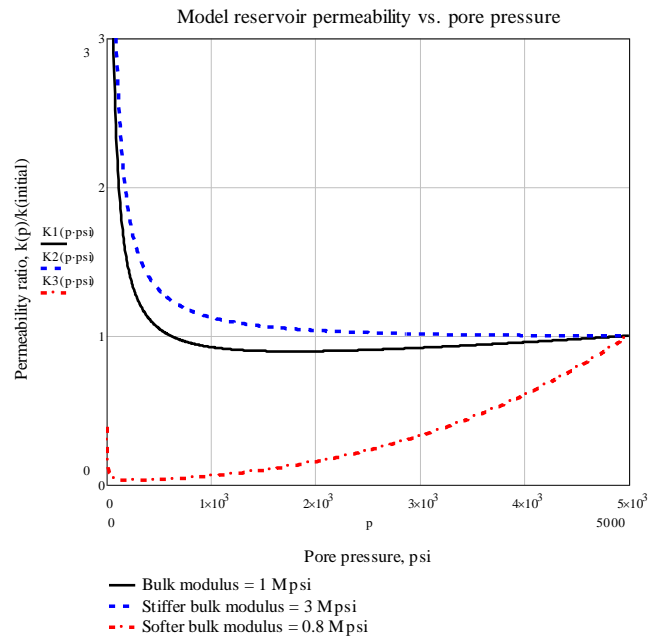


Figure 7. Permeability vs. pressure for different values of bulk modulus K_m .

IV. CONCLUSION

- Stress and pore pressure dependence of permeability is needed for:
 - Adequate drawdown management – not to collapse porosity and permeability near the well during well ramp-up;
 - Estimation of permeability evolution during depletion.

- Based on these reasons a new permeability model of shale gas with two solid porous constituents is derived; the model captures dependence on stress and pore pressure. Stress and pore pressure dependence brings three additional dimension-less parameters, f , γ_m , γ_b , eqs. (4) - (12) which are explicitly expressed through poroelastic mechanical properties of both phases.
- The model predicts existence of compaction-induced minimum of permeability as a function of pore pressure. There is no minimum of permeability with pore pressure decrease in sufficiently stiff formations.
- Dependence of permeability vs. stress and pore pressure, given by Figures 6, 7, is in qualitative agreement with experimental results [9, 10].
- More measurement of permeability as a function of stress and pore pressure are needed to have necessary input parameters and verify the model.

REFERENCES

- [1] F.A.L. Dullien, *Porous Media. Fluid Transport and Pore Structure*, Academic Press, 1992.
- [2] Ph. Charlez. *Rock Mechanics*, v. 1, 2. Paris: Technip, 1991.
- [3] Berryman, J.G., G.W. Milton, 1991. "Exact results for generalized Gassmann's equations in composite porous media with two constituents", *Geophysics*, v. 56, no 12, pp. 1950-1960.
- [4] J.W. Rudnicki, Alteration of regional stress by reservoirs and other inhomogeneities: Stabilizing or destabilizing? *Proc. 9th Int. Con. Rock Mech.*, v. 3, 1629-1637, Paris, France, Balkema, 1999.
- [5] J.B. Walsh. Subsidence above a planar reservoir, *J. Geoph. Res.*, v. 107, no. B9, p. 2202, 2002.
- [6] R.M. Christiansen *Mechanics of Composite Materials*, John Wiley & Sons, New York, 1979.
- [7] M.B. Geilikman, J.M. Karanikas, Sau-Wai Wong. Permeability Model of Shale Gas Rock With Variable Solid Mass, Paper ARMA 13-349, *47th US Rock Mechanics / Geomechanics Symposium*, San Francisco, CA, USA, 23-26 June 2013, 2013.
- [8] M.D. Zoback, and J.D. Byerlee, Permeability and Effective Stress: *AAPG Bulletin*, v. 59, p. 154-158, 1975.
- [9] R. Heller, M. Zoback, Laboratory Measurements of Flow in Gas Shales, *Stanford Rock Physics & Borehole Geophysics*, Meeting 2012, Paper G9, Stanford University, 2012.
- [10] J.P. Vermeylen, "Geomechanical Studies of the Barnett Shale, TX, USA", PhD Thesis, Stanford University, 2011.
- [11] D.S. Scott, F.A.L. Dullien. 1962. Flow of Rarefied Gases. *AIChE Journal*, v. 8, no.3, pp. 293-297.
- [12] S. Otani, N. Wakao, J.M. Smith. 1965. Part II. Diffusion and Flow in Porous Catalysts. *AIChE Journal*, v. 11, no.3, pp. 439-445.



Reliability analysis of complex limit states of floating wind turbines

漂浮风力涡轮机复杂极限状态的可靠性分析

Athanasios Kolios*, Michael Borg, Dawid Hanak

Division of Energy and Power Engineering, School of Engineering, Cranfield University, UK

a.kolios@cranfield.ac.uk

Accepted for publication on 23rd December 2014

Abstract - Offshore wind turbines are developing at a rapid pace and deployments are moving to deeper waters constituting floating support structures as a feasible option both technically and economically at depths that exceed 50 m. Experience of more than 50 years from the Oil & Gas industry has provided structural configurations and established methodologies and standards for the design of floating support structures with varying level of applicability to offshore wind applications, however, the different nature of loading that include a significant operational cyclic loading in addition to the environmental loads, the fact that those structures are designed for volume manufacturing and their limited consequences in the case of failure suggest a probabilistic approach to design and analysis as a pertinent practice towards cost reduction of capital expenditure and operational management. This paper presents a systematic methodology for reliability analysis of the floating support structures, focusing on the case of the analytical derivation of a fundamental limit state for stability under stochastic model inputs that can predict very small probabilities of failure.

Keywords –Offshore wind turbines, floating support structures, reliability analysis, limit states

I. INTRODUCTION

With the need to increase renewable energy's share in global energy production and to exploit offshore wind resources, wind farms are moving further and further offshore into deeper waters. In water depths greater than 50 meters, bottom-mounted (i.e. fixed) support structures for offshore wind turbines do not remain the most economically viable option [1]. A transition from fixed to floating support structures is essential for deep offshore wind farms to become economically viable in the near future.

Whilst it is beneficial to utilize experience from the oil & gas industry during the design and manufacturing of floating wind turbines, the different nature of loading that include a significant operational cyclic loading in addition to the environmental loads, and the fact that those structures are

designed for volume manufacturing and their limited consequences in the case of failure suggest a probabilistic approach to design and analysis as a pertinent practice towards cost reduction of capital expenditure and operational management. In addition to that, the harsh offshore environments are characterized by highly stochastic variables which should be systematically incorporated to the design process in order to avoid accumulation of unnecessary conservatism which ultimately increases total cost.

This paper presents a systematic methodology for reliability analysis of floating support structures, focusing on the case of the analytical derivation of a fundamental limit state for stability under stochastic model inputs able to predict very small probabilities of failure. A sensitivity analysis of the solution based on First Order Reliability Methods (FORM) as well as variation of the statistical properties of the variables that are modelled stochastically, illustrates the performance of the limit state derived for probabilistic analysis. Applicability of the methodology can be extended to other limit states, such as mooring line design and incorporation of coupled dynamics of the complex system as well as inform the requirements for inspection, maintenance, or operational control based on the current state of the structural system.

II. FLOATING WIND TURBINES

The trend so far has been to 'marinise' the optimal onshore configuration (that is, the 3-bladed horizontal axis wind turbine (HAWT)) for use in floating offshore applications. The operating environments found in onshore and floating offshore applications are significantly different, and hence the optimal wind turbine configuration may not be the same for both cases. An alternative to the HAWT that may be more suited to floating applications is the vertical axis wind turbine (VAWT). Although it may have lower individual turbine power coefficients, the generator and transmission machinery is found at the base of the turbine (rather than at the top of the tower for the HAWT) resulting in a lower centre of gravity.

Furthermore a VAWT generates smaller thrust forces and overturning moments than a HAWT, resulting in a smaller support structure being required as compared to a similar-sized HAWT [2].

Following on from the oil & gas industry, the three main types of floating support structures envisaged for floating wind turbines are semi-submersible, spar and tension-leg-platform that achieve stability mainly through buoyancy/waterplane area, ballasting and mooring lines, respectively. In the pursuit of reducing capital and operating costs, a number of concepts have been proposed that are a hybrid of some of the above mentioned platforms, for example, the tension-leg-buoy that combines a spar with a taut mooring system. Likewise a semi-submersible could also have a hybrid slack and taut mooring system to maximize the advantages of each type.

In this paper two floating VAWTs shall be considered, utilizing the spar and semi-submersible floating support structures as presented by Borg and Collu [3], and depicted in Fig. 1.

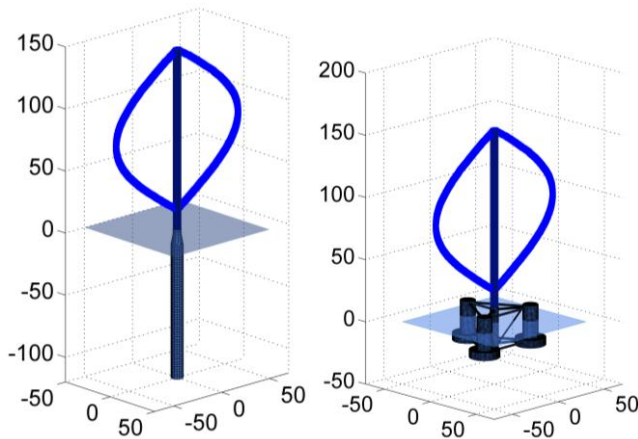


Fig.1: Left – spar-type floating VAWT; Right – Semi-submersible floating VAWT.

III. CAPSIZING LIMIT STATE FOR FLOATING WIND TURBINES

During the preliminary design of the floating support structure, one of the design drivers is the system restoring stiffness in the pitch to counteract the pitch overturning moment generated by the wind turbine. For a moored floating structure, this restoring stiffness is a combination of hydrostatic and mooring system stiffness in pitch [4]:

$$C_{55} = C_{55}^h + C_{55}^m$$

The pitch hydrostatic stiffness is directly related to the metacentric height of the floating structure, and is given by the following equation [5]:

$$C_{55}^h = \rho g V (GM_L)$$

where ρ is the fluid density, g is the acceleration due to gravity, V is the displaced volume of fluid by the structure, and GM_L is the longitudinal metacentric height which is given by:

$$(GM_L) = (KB) + (BM_L) - (KG)$$

where KG is the distance of the centre of gravity from the bottom of the structure, KB is the center of buoyancy from the bottom of the structure, and BM_L is the distance between the center of buoyancy and metacenter, and is given by:

$$(BM_L) = \frac{I_L}{V} = \frac{\iint x^2 dA}{V}$$

where I_L is the second moment of area of the waterplane area of the floating platform. The mooring pitch stiffness is obtained as a product of the surge mooring stiffness and the moment arm of the mooring surge line of action to the center of flotation.

The capsizing limit state can be established by identifying the maximum allowable pitch displacement of the floating wind turbine, ξ_5 , such that the minimum required pitch restoring stiffness, $C_{55,min}$, is identified based on the maximum excitation moment, F_5 [4]:

$$C_{55,min} = \frac{F_5}{\xi_5}$$

Thus the limit state function is defined as:

$$C(X) = C_{55} - C_{55,min}$$

and the zones defined by the limit state function are:

$C(X) > 0$	Failure Region
$C(X) < 0$	Safe Region
$C(X) = 0$	Critical Region

IV. CONCEPTS OF RELIABILITY & PROBABILISTIC ANALYSIS

A reliability analysis of the structural designs is a systematic approach that allows evaluating the levels of safety and serviceability of the structure subjected to the uncertain input. Recently, such methodology has been established as an essential tool in analysis of the actual performance of the structures. Additionally, it formed the basic background for the structures design standards [6].

To determine the structure operability limits, this methodology assumes that the reliability of structures can be estimated based on the limit state function which captures the performance of the structure under loading. A condition under which the structure or its component does not satisfy its design requirements is called a limit state [7]. Each limit state can be characterized by n structure variables, X_i , which affects the structure response. A stochastic representation of these variables needs to be determined. Hence, following the mathematical notation, the limit state can be described as:

$$Z = g(X_1, X_2, \dots, X_n)$$

The critical value for the limit state, which distinguishes the safe and the failure region, is defined as:

$$Z = 0$$

Using the full distributional integration, the probability of failure can be computed within the integration limit of $Z < 0$ using the following equation:

$$P_f = \int \dots \int_{g(x_1, x_2, \dots, x_n) < 0} f_x(x_1, x_2, \dots, x_n) dx_1 dx_2 \dots dx_n$$

where $f_x(x_1, x_2, \dots, x_n)$ is the joint probability density function of the random variables (X_1, X_2, \dots, X_n) . As its accurate estimation requires a complex procedure, indirect methods, such as Monte Carlo simulation, are frequently applied. In the reliability analysis, the probability of failure P_f is often represented in terms of the reliability index β :

$$P_f = 1 - \Phi(\beta)$$

Where the notion Φ is the inverse cumulative distribution function of the normally distributed reliability index.

The integration can be simplified by linearization of the limit state functions using Taylor series expressions. In First Order Reliability Methods (FORM), such as Hasofer-Lind method [8], which use first order Taylor series expression, the reliability index is approximated geometrically in an iterative process as the shortest distance between the limit state surface and zero point of the normalized U-dimensional space. This method, however, would produce inaccurate results if the limit state function is non-linear or has multiple minimal distance points. To enhance the accuracy and reliability of the prediction, the Second Order Reliability Methods (SORM), which use second order Taylor series expression, are also used. In this method, the reliability index is the shortest distance between the limit state function and an asymptotic curve rather than a straight line [9].

V. NUMERICAL ANALYSIS: A CASE STUDY

Table 1: VAWTs design characteristics.

Parameter	Spar-type VAWT	Semi-submersible VAWT
Pitch mooring stiffness (Nm/rad)	311100000	87300000
Pitch hydrostatic stiffness (Nm/rad)	1.0447e+09	7.8780e+08
Buoyancy force (N)	80736300	139939650
Draft (m)	120	20
Mass (tn)	8125.2	14108
Centre of buoyancy (m)	57.863	6.813
Centre of gravity (m)	45.37	11.07
Outer radius (m)	4.8	3
Inner radius (m)	0	0
Cut-off wind speed (m/s)	25	25
Extreme wind speed (m/s)	45.1	45.1
Density (kg/m ³)	1025	1025

Having defined a general form of the limit state functions, these are used to assess the probability that the system is not capable of restoring stiffness in pitch to counteract the pitch

overturning moment generated by the wind turbine. As mentioned above, two floating VAWTs, the characteristic of which is presented in Table 1, are considered.

In this analysis, three variables (pitch mooring stiffness, extreme wind speed and density) are treated stochastically. Due to uncertain nature of wind and wave loads, the coefficient of variation (COV) for wind speed and the pitch mooring stiffness is assumed to be 30% and 50 %, respectively. Conversely, the COV for the water density is assumed to be 10 %. For the sake of this analysis, it is assumed that these variables are normally distributed. The excitation moment has been calculated based on the VAWT characteristics, which is the same for both structures, and is expressed as a second order polynomial function of the wind speed as:

$$F_5 = 4077v^2 + 2.218 \cdot 10^{-9}v - 4.182 \cdot 10^{-8}$$

Moreover, the maximum allowable pitch displacement for the considered VAWTs is assumed to be 10°.

The reliability index was estimated using the iterative Hasofer-Lind method, which is one of the FORM methods.

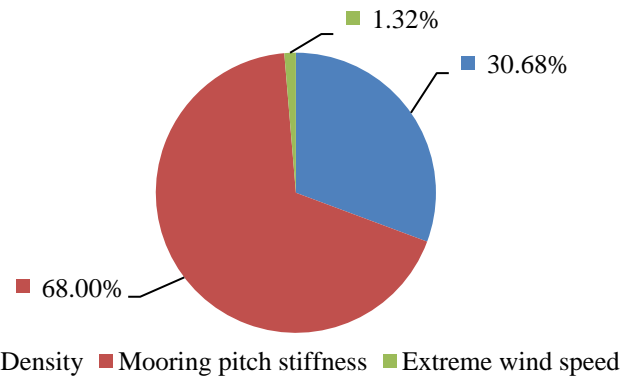


Fig. 2: Importance factors of the stochastic variables in estimation of the reliability index for the spar-type floating VAWT.

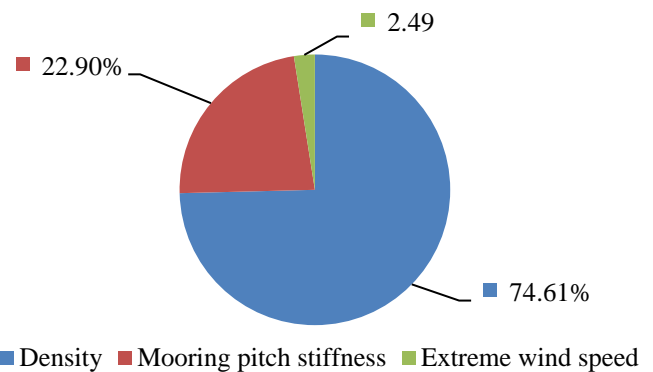


Fig. 3: Importance factors of the stochastic variables in estimation of the reliability index for the semi-submersible floating VAWT.

From Fig. 2 it is clear that in the spar-type floating VAWT the variation in the pitch mooring stiffness has the highest effect on the reliability index, right after the water density. Conversely, as shown in Fig. 3, the reliability index for the semi-submersible floating VAWT is mostly affected by the

water density. This means that the effect of the wave loads on the mooring pitch stiffness is partially avoided for the semi-submersible floating VAWT. However, this kind of VAWT is more prone to be affected by the wind loads, what is indicated by higher contribution of the extreme wind speed in the reliability index compared to the spar-type floating VAWT.

Table 2: Reliability analysis results.

Parameter	Spar-type VAWT	Semi-submersible VAWT
Reliability index β	6.92	8.95
Probability of failure P_f	2.24e-12	0

The results of the conducted analysis presented in Table 2 indicate that the reliability index for both structures is high. This means that the probability of the structure overturning due to variation in the wind and wave loads, as well as water density, is negligible. The analysis also showed that the semi-submersible floating VAWT would provide better performance in terms of system reliability. This probably results from the lower impact of the mooring pitch stiffness on the reliability index as identified above.

VI. CONCLUSION

This paper presents a methodology for the reliability analysis of two kinds of floating support structures for VAWTs. The VAWTs background study is followed by a description and derivation of the capsizing limit state for the floating wind turbines. Next, the stability check is conducted through estimation of the reliability indices, and thus the failure probabilities, for the spar-type and the semi-submersible floating VAWTs. The analysis showed that the impact of the mooring pitch stiffness on the reliability of the structures is reduced for the semi-submersible floating VAWTs, at an expense of the wind speed. Nevertheless, application of such structure would result in increased reliability index, hence in lower probability of the structure overturning. Finally, a simplified model for coupling of the aero-hydro-servo-elastic induced dynamics of a VAWT and its effect on reliability estimation has been proposed.

REFERENCES

[1] Collu, M., Kolios, A. J., Chahardehi, A. and Brennan, F. "A comparison between the preliminary design studies of a fixed and a floating support structure for a 5 MW offshore wind turbine in the north sea", RINA, Royal Institution of Naval Architects - *Marine Renewable and Offshore Wind Energy - Papers*, pp. 63, 2010.

[2] Borg, M., Collu, M. and Brennan, F. P. "Offshore floating vertical axis wind turbines: advantages, disadvantages, and dynamics modelling state of the art", *The International Conference on Marine & Offshore Renewable Energy (M.O.R.E. 2012)*, 26-27 September, 2012, London, RINA.

[3] Borg, M., Collu, M. "A comparison on the dynamics of a floating vertical axis wind turbine on three different floating support structures", *11th Deep Sea Offshore Wind R&D Conference*, 22-24 January, 2014, Trondheim, Norway.

[4] Wayman, E. N., *Coupled Dynamics and Economic Analysis of Floating Wind Turbine Systems*, 2006, MSc Thesis Massachusetts Institute of Technology, Cambridge, USA.

[5] Fossen, T.I. *Handbook of Marine Craft Hydrodynamics and Motion Control*, 2011, Wiley.

[6] DNV, T.I. *Guideline for Offshore Structural Reliability Analysis – General*, 1995, DNV Report No: 95-2018, Det Norske Veritas.

[7] DNV, *DNV Offshore Standard OS-C101: Design of offshore steel structures, General – LRFD Method*, 2008, Det Norske Veritas

[8] Hasofer, A. M. and Lind, N. C., "Exact an Invariant Second Moment Code Format", *Journal of the Engineering Mechanics Division*, 1974, ASCE

[9] Kolios, A. J., Collu, M. and Brennan, F. P., "Reliability of Floating Foundation Concepts for Vertical Axis Wind Turbines", *The 11th International Symposium on Practical Design of Ships and Other Floating Structures (PRADS)*, 2010

NOMENCLATURE

BM_L	Distance between the center of buoyancy and metacenter
C_{55}	System restoring in pitch
C_{55}^h	System hydrodynamic pitch stiffness
C_{55}^m	System mooring pitch stiffness
F_5	Steady state excitation moment
g	Gravitational acceleration
GM_L	Longitudinal metacentric height
I_L	Second moment of area of the waterplane area of the floating platform
KB	Centre of buoyancy from the bottom of the structure
KG	Distance of the center of gravity from the bottom of the structure
P_f	Probability of failure
v	Wind speed
V	Fluid volume displaced by the structure
X_i	Random variables
Z	Limit state function
β	Reliability index
ζ_5	System steady state pitch
ρ	Density



Fleet monitoring for distributed energy systems

分布式能源系统的车队监测

Marc Hilbert*, Tobias Vraetz, Andrea Kulanthavadeivel, Karl Nienhaus

Institute for Mining and Metallurgical Machinery, RWTH Aachen University, Aachen, Germany

mhilbert@imr.rwth-aachen.de

Accepted for publication on 23rd December 2014

Abstract – Distributed energy systems such as wind turbines or tidal power systems share the properties of (1) having a rising number of similar installed system setups, (2) being installed mostly in remote areas with limited access and (3) needing a high system reliability. This makes fault diagnosis and identification (FDI) a crucial but challenging part for operation and maintenance (O&M) of these systems. This paper will focus on a method to use condition information of equal components in different machines and under different working conditions, to extract useful information for FDI of those components. A definition for fleet monitoring for FDI will be introduced. It will be shown that by extracting specific features of the components condition information and by combining these features from different machines, additional FDI information can be gained. Therefore, the focus of data analysis is the fleet information and less only individual systems information. It will be shown that properties of the introduced method can resolve common FDI drawbacks, e.g. setting up alarm thresholds. The method is based on the calculation of selected features from each system in a high dimensional common feature space. The main advantage is the absence of absolute measures for FDI and use of relative measures between components/machines in the fleet. Besides the theoretical approaches, an example using temperature and vibration data of 17 bearings test runs (PRONOSTIA data set) will be given. The runs of the bearings were performed with different speed and load and were only stopped by significant degradation. The purpose of the paper is to increase system reliability by using fleet information and, therefore, provide additional information for FDI.

Keywords – Fleet Monitoring, Condition Monitoring, Energy Systems, Bearing, Multivariate normal distribution

I. INTRODUCTION

Worldwide an increasing demand for energy can be observed. More than 80 % of global energy, which is generated from renewable source, is hydro power. In addition to that the annual increase is approximately 3 %. There are considerable opportunities for hydroelectric plants, since only one fifth of technical feasible potential of hydro power has been deployed. North America utilized the biggest potential of hydro power, approximately 33 %, followed by Europe including the CIS 30 %, Australia 27 %, Asia 23 % and finally Africa with the lowest percentage of 8 %. [1] [2]

Mostly distinction is made between run-of-the-river power plant, storage power plant, pumped storage hydro power station and tidal power plant. The run-of-the-river power plant uses the flow of the river to generate electricity and also low drop height is characteristic. Storage power plants certainly have a high gradient and use the storage capacity of dams to generate electricity. A big advantage of storage power plants is that they are both used to cover the electrical base load and peak-load operation. The pumped storage power plant also offers the capability to pump the water into a catch basin. To allow this, the energy, which is available when demand is low, is used for example at night. At peak times, electricity can be feed in again. The tidal power plant converts the potential and kinetic energy from the tides of the sea into electricity. They are built in bays and estuaries, which have a particularly high tide.

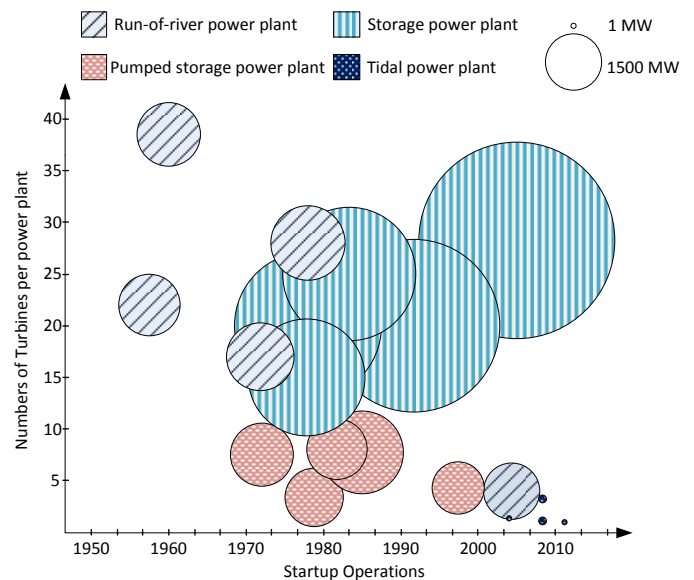


Fig. 1. Selection of hydro power plants.

Fig. 1 and Table 1 show the different types of hydroelectric plants. For each type the world's largest power plants are listed. Furthermore the diagram shows when the hydro power plants were put into operation and how many turbines were installed. The bigger the circles, the more total power output

the individual power plants have. It is particularly interesting to note that tidal power stations are typically equipped with rolling bearings, in contrast to the other types of power plants, which have almost exclusively plain bearings. Tidal energy systems are similar to all distributed energy systems such as on- and offshore wind turbines, communal power stations, waste-to-energy power stations and others. Distributed power system combine the following properties relevant for O&M: (1) having a rising number of similar installed system setups, (2) being installed mostly in remote areas with limited access and (3) needing high system reliability.

Using the introduced example of water power plants shown in Fig. 1 in all major power plants the turbines are concentrated in one place even in one machine hall. Therefore the mentioned O&M properties do not apply. By looking at the tidal power plants and referring to the defined O&M properties: (1) tidal power plants are installed in clusters of similar machines and run under similar stream/tidal conditions, (2) each turbine is located separately underwater and therefore requires increased effort to be accessed and (3) are designed to run without onsite support for 6 months [3].

TABLE 1: SELECTION OF HYDRO POWER PLANTS.

Name of power plant	Country	Startup Operation	Numbers of turbines per power plant	Total power output [MW]
Run-of-river-power plant				
Chief Joseph Dam	USA	1979	27	2620
John Day Dam	USA	1971	16	2160
Beauharnois Hydroelectric Power Station	Canada	1961	38	1903
The Dalles Dam	USA	1957	22	1.780
Nathpa Jhakri Dam	India	2004	6	1.500
Pumped storage power plant				
Bath County	USA	1985	6	3.003
Ludington	USA	1973	6	1.872
Dinorwig	Great Britain	1984	6	1.728
Racoon-Mountain	USA	1978	4	1.600
Shin-Takasegawa	Japan	1998	4	1.280
Storage power plant				
Three Gorges Dam	China	2006	26	18.200
Itaipú	Paraguay and Brazil	1991	20	14.000
Guri	Venezuela	1978	20	10.235
Tucuruí	Brazil	1984	25	8.370
Sayano-Shushenskaya Dam	Russia	1978	8	6.400
Tidal power plant				
RTT 2000	Wales	2011	1	2
SeaGen	UK	2008	2	1.5
OCT	Scotland	2008	1	1.5
TidEl	Cumbria	2005	2	1

By knowing these challenging properties most of the distributed energy systems are equipped with remote condition monitoring systems measuring e.g. vibration to estimate the

condition of the system and sending the data to a centralized control center. At those centers the data is analyzed and O&M measures are decided.

The purpose of the paper is to increase system reliability by using fleet information and, therefore, provide additional information for O&M. First the problem of fleet monitoring will be introduced (II), then the proposed method is described (III) and later demonstrated using bearing data (IV).

II. PROBLEM DEFINITION

The problem that is researched in this paper is defined as supporting the monitoring effort of distributed energy system based on existing machine data. The focus is to detect unusual machine behavior.

For this purpose the authors define the term fleet monitoring as: *Monitoring a fleet of similar type or identical machines, operating under similar conditions, to detect unusual machine behavior of a single machine if compared to the fleet.* Additionally the introduced fleet monitoring method makes no use of design specific quantitative thresholds and no use of historical monitoring data. The focus is not on machine individual FDI or prognosis of future machine conditions.

III. THEORETICAL APPROACH

The method of fleet monitoring is presented with the focus on roller bearings and assumes that acceleration over time data of a machine fleet is available.

Features

At first k features of m separate bearings B_m of m machines of the machine fleet for n time intervals (of equal length) are extracted (Fig. 2) resulting in values defined as $f_{k,n,m}$. In this paper the root mean square (RMS), the peak magnitude to RMS ratio (Peak2RMS) and the maximum to minimum difference (Peak2Peak) are used [4].

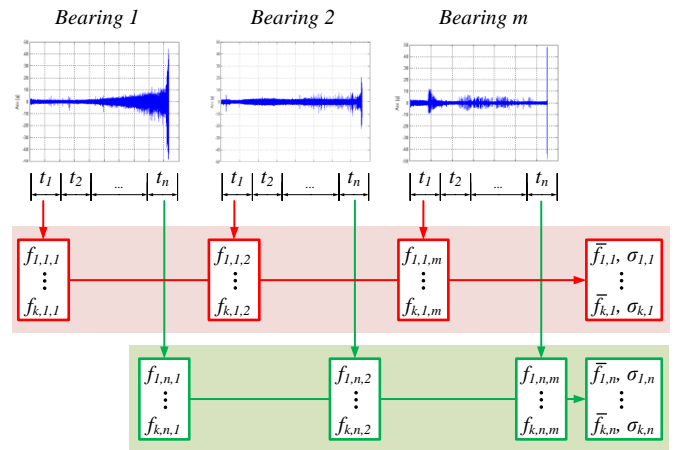


Fig. 2, Feature extraction method.

Test of normal distribution

For each time interval n all extracted features $f_{k,n,m}$ are tested if the features in that specific time interval are normal distributed. Therefore the Anderson–Darling test with a significant level of 5 % is used. This test was chosen because of its capability to test a small sample size. The test is valid

until a sample size of at least 8. Therefore a machine fleet of less than 8 machines cannot be assumed normal distributed and therefore not monitored with the method of this paper. [5]

Only if all features k are normal distributed for a specific time interval n , their mean values $\bar{f}_{k,n}$ (Eq. 1) and their standard deviations $\sigma_{k,n}$ (Eq. 2) are calculated.

$$\bar{f}_{k,n} = \frac{1}{m} \sum_{i=1}^m f_{k,n,i} \quad (1)$$

$$\sigma_{k,n} = \sqrt{\frac{1}{m} \sum_{i=1}^m (f_{k,n,i} - \bar{f}_{k,n})^2} \quad (2)$$

Multivariate normal distribution

The core method for fleet monitoring is the multivariate normal distribution (also called multivariate Gaussian distribution). It is a multi-dimensional type of univariate normal distributions. Fig. 3 illustrates an example of a two-dimensional normal distribution for a specific time interval n . The abscissa and ordinate axis display two different features (f_1 , f_2), their mean values ($\bar{f}_{1,n}$, $\bar{f}_{2,n}$) and their standard deviations ($\sigma_{1,n}$, $\sigma_{2,n}$) as characteristic values for a standard normal distribution. It is important to note that the representation is valid for only a single time interval. Another time interval is checked separately from all other time intervals. [6]

If the criterion on normal distribution of every feature is fulfilled, the original values of every dataset are compared to the statistically calculated multidimensional values $\bar{f}_{k,n}$ and $\sigma_{k,n}$. The calculated (double) standard deviations of each feature are then used as thresholds ($2 \cdot \sigma_{k,n}$) which equals 95.45 % of the distribution. The features $f_{k,n,m}$ of each bearing B_m are then compared to the $2 \cdot \sigma_{k,n}$ threshold of the specific time interval n . If all $f_{k,n,m}$ of each bearing B_m are not within this range of tolerance, the bearing could be classified as a bearing with unusual behavior.

In Fig. 3 an example with just two features, f_1 and f_2 , and $m=8$ Bearings for specific time interval is given. It can be seen that the bearings B_1 to B_4 are all within the tolerated range of all features. In contrast, bearings B_5 and B_6 are neither within the tolerated range of f_1 nor f_2 indicating that these bearings might have a unusual behavior. Nevertheless, bearings B_7 and B_8 are not within the tolerance of single features. Bearing B_7 is only within the tolerated range of f_2 and bearing B_8 is only within the tolerated range of f_1 . Therefore, both bearings are classified as having usual behavior.

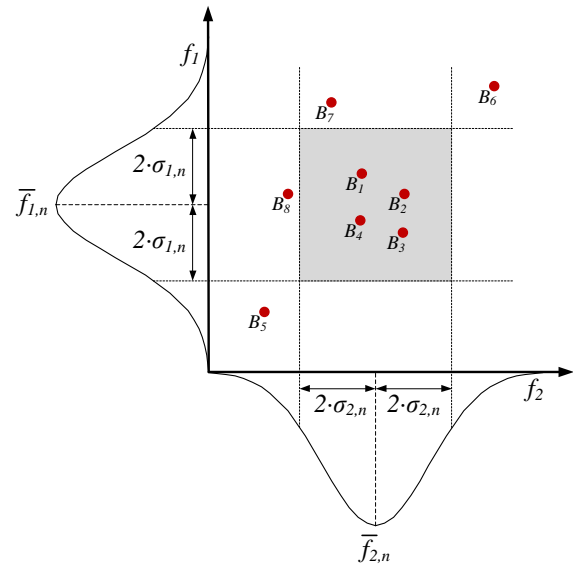


Fig. 3, Two-dimensional normal distribution for time interval n .

IV. APPLICATION

Data description

For the multivariate analysis of the above described features, an already existing dataset was used. The dataset descends from the FEMTO-ST Institute (Besançon, France) which has done experiments on their laboratory experimental platform named PRONOSTIA for a bearings' life duration prognostic challenge called "IEEE PHM 2012 Data Challenge" (in the following referred to as Challenge) [7]. The objective of the laboratory platform is to provide real experimental datasets in a short time. The data describes failures of ball bearings during their different operating times.

The published datasets of the Challenge represent three different load cases. Within the first load case, in total seven bearings were damaged at $1,800 \text{ rpm}$ and a force of 4.0 kN . Additionally, seven bearings were provoked to reach failure at $1,650 \text{ rpm}$ and 4.2 kN . The last load stage was $1,500 \text{ rpm}$ and 5.0 kN . Three bearings were experimentally tested under this determined condition. The test was stopped when the amplitude of the bearing vibration signal exceeded 20 g . During the experiments, a tenth of a second of horizontal and vertical vibration signals were recorded each 10 seconds at a sample frequency of 25.6 kHz . The first trial of fleet monitoring for these bearings is based on the features of the horizontal vibration signal because the load was applied in horizontal direction. The previously described features of the horizontal vibration signal of 17 bearing datasets were analyzed within this paper.

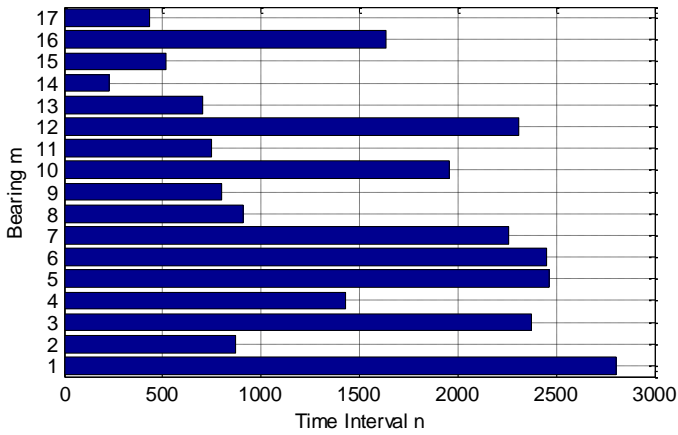


Fig. 4, Available time intervals n for all 17 bearings.

Results

The available time intervals n for each bearing m is shown in Fig. 4. Because of a minimum of at least 8 required bearings, to assure test for normal distribution, the method will not deliver a result after the end of the life time of bearing $m=16$ at time interval $n=1637$. It has to be noted that always all bearings m are tested of each time interval n , assuming that all bearings started operating at $n=1$.

The method is implemented as described in section III and was tested with the introduced data set. Fig. 5, 6, 7 and 8 shows the result of 4 selected bearings for a three dimensional normal distribution. The normal distributed features (RMS, Peak2RMS and Peak2Peak) over time intervals are plotted for the bearings $m=4, 9, 16$ and 17 . The ordinate axis represents the ratio defined in Eq. (3):

$$ratio_{k,n,m} = \frac{|f_{k,n,m} - \bar{f}_{k,n}|}{\sigma_{k,n}} \tag{3}$$

Also marked is the $2 \cdot \sigma_{k,n}$ threshold. If two features exceed this threshold in the same time interval an unusual behavior is detected. The results of all 17 bearings are summarized in Table 2. It has to be noted that the grey marked bearings are the ones where the criteria of at least 8 bearings in the fleet is not fulfilled anymore therefore the method of this paper cannot be applied. This is due to the fact that always the same n of all bearings is compared and that each bearing has an individual life span. Therefore a bearing that is considered damaged by [7] does not have any further measurements and falls out of the fleet. Additionally Table 2 shows in percentage when the unusual behavior was detected as a fraction of the total number of measured time intervals n .

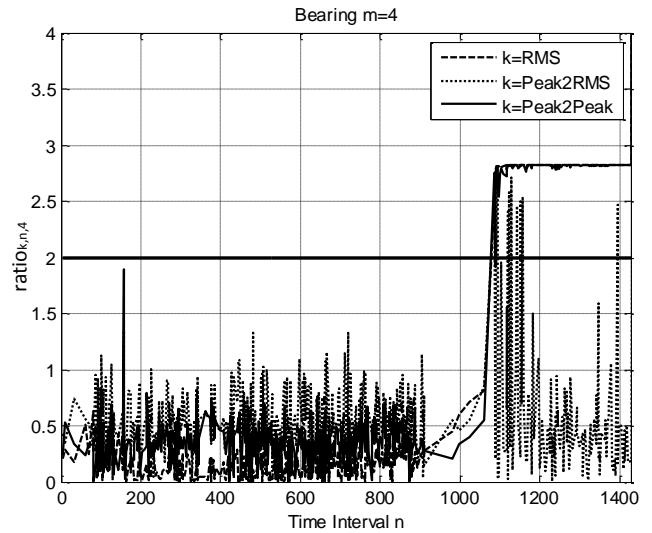


Fig. 5, Feature distribution ratio of bearing $m=4$.

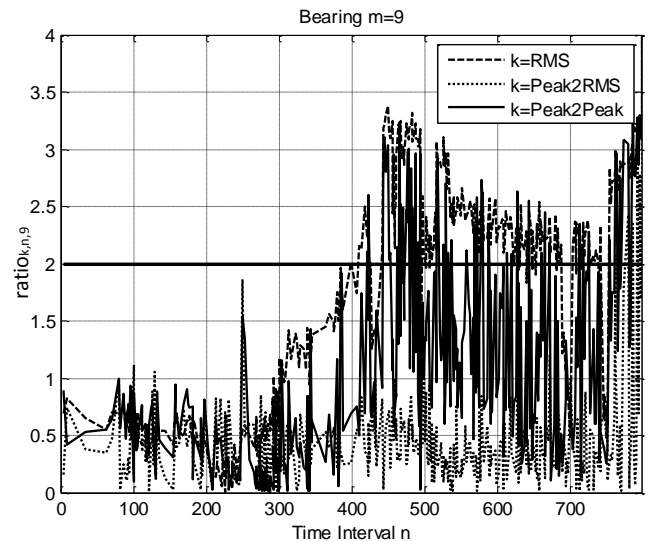


Fig. 6, Feature distribution ratio of bearing $m=9$.

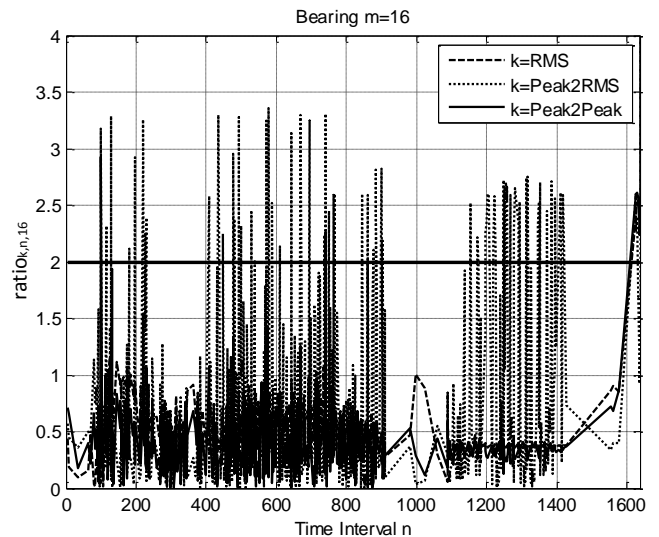


Fig. 7, Feature distribution ratio of bearing $m=16$.

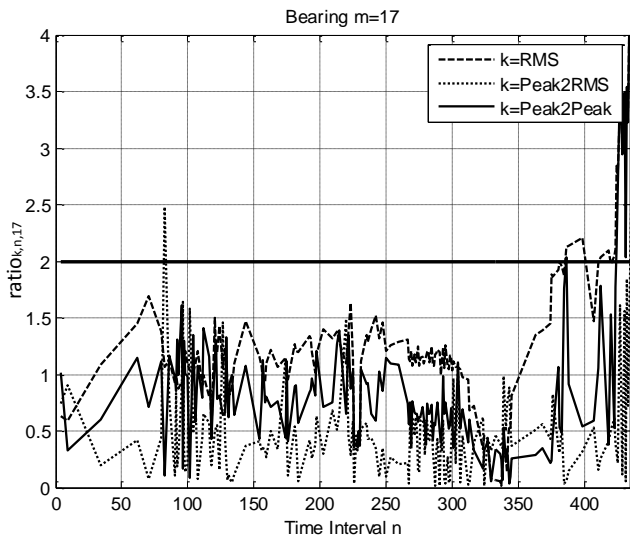


Fig. 8, Feature distribution ratio of bearing $m=17$.

Discussion

It can be seen that for all normal distributed bearings an unusual behavior before the end of life time could be classified using no design specific quantitative thresholds. Bearing $m=2$, 8, and 16 show a very early detection of fewer than 6% of the total bearing life time. An early classification is not a desired result because in this early state of the total life time of the bearing the behavior should be still considered as usual behavior. By comparing the early detection of bearing $m=16$ with Fig. 7 it can be seen that this is due to noisy Peak2RMS and Peak2Peak features. It also can be seen that at the end of the bearing life time a usual behavior was also classified. Therefore further investigations should be done to lower the impact of noisy features. This fact shows the dependency of selected features of the method.

TABLE 2: SUMMARIZED RESULTS FOR ALL 17 BEARINGS.

Bearing m	Nb. of measured intervals n	Nb. of normal distributed intervals	Interval of fist unusual behavior	Percentage of life time
1	2803	620	-	-
2	871	444	6	1
3	2375	620	-	-
4	1428	607	1087	76
5	2463	620	-	-
6	2448	620	-	-
7	2259	620	-	-

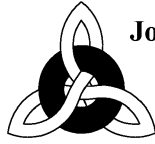
8	911	470	34	4
9	797	399	420	53
10	1955	657	-	-
11	751	370	745	99
12	2311	620	-	-
13	701	337	693	99
14	230	70	104	45
15	515	221	491	95
16	1637	620	100	6
17	434	165	386	89

V. CONCLUSION

In this paper a method for fleet monitoring is given to detect unusual machine behavior of a single machine if compared to the fleet. The method is applied to vibration data of 17 bearings. For a fleet size of at least 8 bearings, for every bearing in this fleet unusual behavior could be detected before the end of the bearing life time. The results show the detectability depending on fleet size and feature selection. Further research regarding a sensitivity analyses, feature extraction and feature interconnectivity is needed.

REFERENCES

- [1] Rieg Frank, S. R. (2012). *Handbuch Konstruktion*. Hanser
- [2] Voith, G. (April 08, 2014). *Voith*. Retrieved May 06, 2014 from: <http://voith.com/de/index.html>
- [3] C.A. Douglas, G.P. Harrison, J.P. Chick “Life cycle assessment of the Seagen marine current turbine”, Proc. IMechE Vol. 222 Part M, 2008, DOI: 10.1243/14750902JEME94
- [4] IEEE® Standard on Transitions, Pulses, and Related Waveforms, IEEE Standard 181, 2003.
- [5] R.B. D’Agostino (1986). "Tests for the Normal Distribution". In D’Agostino, R.B. and Stephens, M.A. Goodness-of-Fit Techniques. New York: Marcel Dekker. ISBN 0-8247-7487-6.
- [6] A. Gut (2009) An Intermediate Course in Probability, Springer. ISBN 9781441901613
- [7] P. Nectoux, R. Gouriveau, K. Medjaher, E. Ramasso, B. Morello, N. Zerhouni, C. Varnier. “PRONOSTIA: An Experimental Platform for Bearings Accelerated Life Test”, *IEEE International Conference on Prognostics and Health Management*, Denver, Colorado, USA, 2012.



Integrated offshore transmission

综合海洋传输

Dr. Biljana Stojkovska*, Faith Natukunda, Sheriff Ilesanmi

National Grid, Warwick, CV34 6DA, UK

Accepted for publication on 24th December 2014

Abstract - Electricity generated from offshore renewable energy sources is expected to make an important contribution towards the UK achieving its renewable energy targets by 2020. The government's Renewable Energy Roadmap (2011) suggests that there could be 11 to 18 GW of offshore wind capacity by 2020. There is also substantial scope for further growth beyond this, with the Crown Estate Round 3 zones representing up to 32GW of additional offshore generation. Achieving such levels will require a timely, cost-effective and secure offshore electricity transmission network to transfer electricity generated offshore to the onshore network.

Up until now, offshore transmission assets have been developed as single, standalone connections to shore ("radial" connections). However, the Round 3 offshore wind projects are larger, more complex and at a greater distance from the shore than those that have been developed to date, and as a result there could be greater potential for network efficiencies through offshore asset integration. This could include integration between connections and coordination between the strategic development of the onshore and offshore networks through offshore reinforcement projects.

This paper will present the benefits of integrated and coordinated offshore designs to help improve boundary capability while incorporating flexibility into the existing transmission network, and providing offshore options to avoid potential delays usually associated with onshore reinforcements. This aims to achieve efficient reinforcement of the wider and local system boundaries for timely connection of offshore projects, helping to meet the government renewable targets while presenting the most economic and efficient outcome for UK consumers. The proposed methodology for optimal offshore integrated design will be applied to offshore connections of Round 3 on the East Coast in Great Britain.

Keywords – National Electricity Transmission (NETS) System Security and Quality of Supply Standards (SQSS), Local System Boundaries, Wider System Boundaries, Integrated Offshore Design, Required Transfer (RT), Boundary Capability (BC)

I. PLANNING OF TRANSMISSION SYSTEM FOR OFFSHORE WIND GENERATION

The government has set an ambitious target for the deployment of renewable energy over this decade culminating

with 15 % of the UK's total energy needs being met from renewable sources by 2020. This means that around 30 % of electricity in Great Britain (GB) may come from renewables. To achieve this substantial deployment of green energy the government has established a policy framework to support investment in renewable generation. Within this framework, offshore wind is recognised as being an important source of renewable energy with financial incentives to encourage further investment. In particular three very large offshore wind power plants are planned for connection on the East Coast of GB namely Dogger Bank, Hornsea and East Anglia.

Connection of these offshore wind power plants will have a significant impact on the development of the transmission network. For the power generated to reach homes and businesses in Great Britain the existing electricity networks must be developed to reflect the change in generation location. A step change in network investment of this kind calls for a more dynamic approach to the development of transmission networks: an open, competitive approach that is built on encouraging innovation and new sources of technical expertise and finance.

National Grid has a statutory duty under the Electricity Act 1989 to develop and maintain an efficient, co-ordinated and economical system of electricity transmission. NGET also has a duty to facilitate competition in the supply and generation of electricity and must offer a connection to any proposed generator. The National Electricity Transmission System (NETS) is designed in accordance with the requirements of the Security and Quality of Supply Standard (SQSS). The standard sets out the minimum requirements for both planning and operating the NETS so that a satisfactory level of reliability and power quality is maintained. Thus any modification to the transmission system, for example new offshore generation connections, external connections and/or changes to demand must satisfy the requirements of the NETS SQSS. The NETS SQSS is applicable to all GB transmission licensees including National Grid, Offshore Transmission Owners (OFTOs) and the Scottish Transmission Owners.

In this paper the concept of Integrated Offshore Transmission is presented to assess the benefit of coordinating onshore and offshore transmission development. Using the

concept of Planned Transfer and assessing Boundary Capability, the effectiveness of integrated onshore and offshore solutions are examined for generation scenarios which reflect the potential build-up of offshore wind power plants at Dogger Bank, Hornsea and East Anglia.

The remainder of this paper is organised as follows: in section II the Methodology and General assumptions are introduced. Section III elaborates the Offshore Integrated Designs. Section IV, the last Section presents the concluding remarks.

II. METHODOLOGY AND GENERATION ASSUMPTION

A. General Methodology

The concept of Required Transfer and Assessment of Boundary Capability is used to identify the need for reinforcement on the Wider System Boundaries and East Coast Local System Boundaries, following this, design options are developed to provide the required capability.

1.1 Boundary Assessment in Transmission Planning

The NETS SQSS specifies separate methodologies for local boundaries and wider boundaries analysis. The differences between both are in the level of generation and demand modelled, which in turn directly affect the level of boundary transfer to be accommodated.

Local Boundaries: The generation is assumed at its registered capacity and the local demand is assumed to be that which may reasonably be expected to arise during the course of a year of operation. Local boundaries must be able to accommodate any generation to be connected without being constrained by the local network in the year of operation.

Wider Boundaries: In the case of wider system boundaries the overall generation is selected and scaled according to the Security and Economic criteria described below and assessed against peak demand, which result is a 'Planned Transfer' level. For each system boundary an interconnection or boundary allowance is calculated and added to the 'Planned Transfer' level to give a 'Required Transfer' level. In this way the standard seeks to ensure that peak demand will be met, allowing for variation in both generator location and demand forecast.

1.2 Wider Boundaries: Security and Economy Criteria

The 'Planned Transfer' of a boundary, as defined by the NETS SQSS, is based on the balance of generation and demand on each side of the boundary and represents the natural flow on the Transmission system for a given demand and generation background and is determined by the geographic location of demand and generation, as well as the impedance of the interconnecting circuits. The 'Required Transfer' of a boundary is the Planned Transfer value with the addition of an interconnection or boundary allowance based on an empirical calculation defined in the SQSS.

The full interconnection allowance is applied for single circuit losses and half the allowance is applied for two circuit

losses. A shortfall in Boundary Capability compared with the Required Transfer indicates a need for reinforcement of that boundary. The SQSS specifies two separate criteria upon which transmission capability should be determined. These are described below and are based on Security and Economic factors respectively.

The Security Criterion:

The object of this criterion is to ensure that demand can be supplied securely, without dependence on intermittent generators or imports from interconnectors. The generation background is set by:

Determining from a ranking order, the conventional generation required to meet

- 120% of peak demand, based on the generation capacity.
- Scaling the output of these generators uniformly to meet demand (this means a scaling factor of 83%).

This selection and scaling of surplus generation takes into account generation availability. Based on this the Planned and Required Transfer values are calculated in the usual way. This criterion determines the minimum transmission capability required, ensuring security of supply. This is then further assessed against the economic implications of a wide range of issues such as safety, reliability and the value of loss of load.

The Economic Criterion:

As increasing volumes of intermittent generation connect to the GB system, the Security Criterion will become increasingly unrepresentative of year-round operating conditions. The Economy criterion provides an initial indication of the amount of transmission capability to be built, so that the combined overall cost of transmission investment and year-round system operation is minimised. It specifies a set of deterministic criteria and background conditions from which the determined level of infrastructure investment approximates to that which would be justified from year-round cost benefit analysis.

In this approach scaling factors are applied to all classes of generation such that the generation meets peak demand. Based on this the Planned and Required Transfer values are calculated in way explained above. If a comparison with the Economy Criterion identifies additional reinforcements, a further cost benefit analysis should be performed in order to refine the timing of a given investment. In networks where there is a significant volume of renewable generation it is expected that the application of the Economy Criteria will require more transmission capacity than the Security Criteria to ensure there is sufficient transmission capacity.

B. East Coast Specific Assumptions

The North Sea has some of the largest proposed offshore generation projects, including the Dogger Bank, East Anglia

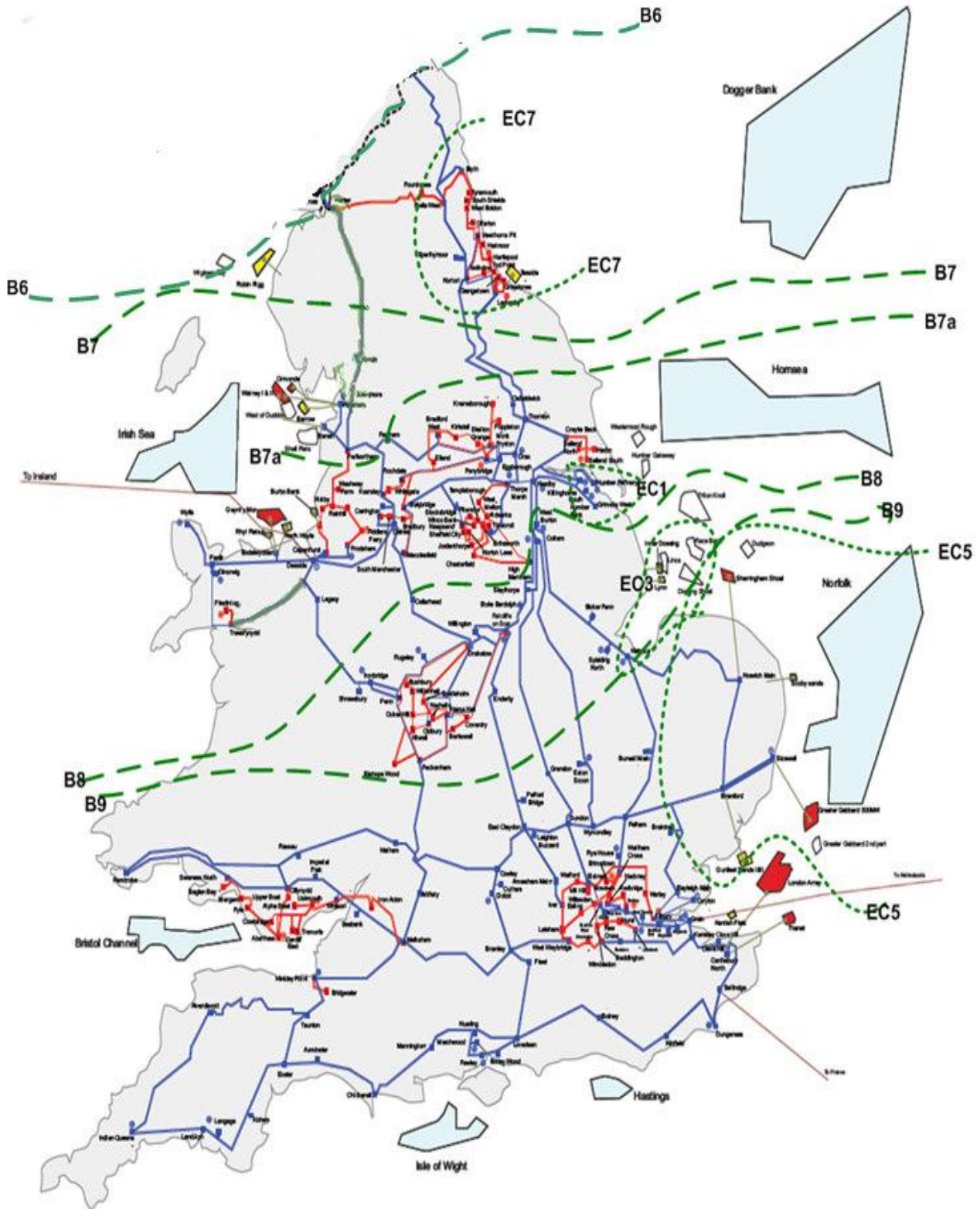


Figure 1. Illustration of Local and Wider System Boundaries

and Hornsea. To assess the impact of offshore wind power plants planned to be connected on East Coast, the following

generation contracted Transmission Entry Capacity (TEC) data are taken into consideration:

- Dogger Bank 6 GW but considered up to 9GW
- Hornsea 4.8 GW
- East Anglia 7.2 GW

A sensitivity scenario is developed that takes into account both the TEC data as well as the published future energy scenarios such as the Gone Green Scenario. Overall there is the potential for over 25 GW of capacity from the East Coast and East Anglia (from the Crown Estate Round 1, 2 and 3 offshore wind farm projects). Connection of these projects to the wider transmission network involves multiple transmission connections all along the East coast from Teesside to the Thames Estuary including areas around Humberside, Lincolnshire and the Wash.

2.1 East Coast Local System Boundaries

These smaller areas of the NETS, which typically contain a large imbalance of generation and demand leading to heavy loading of the circuits crossing the boundary. As demand is not predicted to change significantly over the period, the local boundaries see significant growth generation and high boundary transfers. The local boundaries (see Figure 1) for the three large East Coast offshore wind power plants are:

- Dogger Bank connecting to local boundary EC1, EC3 and EC7
- Hornsea connecting to local boundary EC1 and EC3
- East Anglia connecting to local boundary EC5

2.2 East Coast Wider System Boundaries

Wider system boundaries are those that separate large areas of the GB transmission system containing significant quantities of demand and generation. With a predominant power flow toward the demand centre of London and the South East, connection of all three wind power plants impact directly boundaries B7, B7a and B8 and indirectly boundaries B6 and B9, presented in Figure 1. These wider system boundaries are analysed to ensure the SQSS requirements are maintained.

Each generation scenario has a corresponding boundary requirement from which the boundary reinforcement needs can be identified.

2.3 East Coast Boundaries Overview

The East Coast transmission network consists of a number of generation groups (Teesside, Humber, and East Anglia) which are connected to the main 400kV system via a strong 400kV spine from Lackenby through Creyke Beck, Keadby and Walpole to Pelham.

Teesside Group (EC7): In addition to the offshore wind, the North East could see the connection of multiple HVDC links from Scotland and an interconnector with Norway. These would result in increased power injections into this region.

The Humber group (EC1) consists of two 400kV double circuit lines running from Keadby towards Killingholme, with one continuing toward Grimsby on the coast. These lines gather outputs of power stations on the south side of the Humber and feed it into the main system at Keadby. From Keadby transmission circuits link the East Coast system via

West Burton, Spalding North, and Bicker Fen into Walpole. There are also significant generation connections at West Burton and Keadby, adding to the power requiring throughout.

The transmission system in the East Anglia area (EC3, EC5) is characterised by a double circuit ring that links Walpole, Norwich, Bramford, Pelham and Burwell Main substations. Pelham substation provides additional interconnection between the East Anglia region and other sections of the transmission system.

C. Boundary Capabilities

For every boundary, the future capability necessary under each scenario is calculated by the application of the security standards and methodology explained above. The network at peak system demand is used to outline the minimum required transmission capability for Economy criteria. The years for consideration are 2021 and 2030.

3.1 Local System Boundaries

3.1.1 Boundary EC1

Boundary EC1 is an enclosed local boundary in the Humber group, consisting of four circuits that export power to the Keadby substation. The maximum power transfer out of this boundary is currently 5.5 GW which is limited by thermal overloads on the boundary circuit. The boundary is at its local limit and any further generation injections would require onshore reinforcement.

3.1.2 Boundary EC3

Boundary EC3 is a local boundary surrounding the Walpole substation and includes the six 400kV circuits out of Walpole. Walpole is a critical substation in supporting significant offshore generation connections and high North-South network power flows along the East Coast network. The maximum boundary transfer capability is currently limited to 3.2GW by thermal overloads on the boundary circuits. Following the Walpole re-build, Walpole will be able to accommodate up to a further 2GW before reaching its limit.

3.1.3 Boundary EC5

The local boundary EC5 covers the Eastern part of East Anglia including the substations of Norwich, Bramford and Sizewell. There is mainly generation enclosed by the boundary so that power is typically exported out of the enclosed zone, predominantly along the southern circuits. The maximum boundary transfer capability is currently limited to 3.4 GW due to thermal overload on the boundary circuits. Several onshore reinforcements are planned to facilitate the rapid build-up expected from East Anglia.

3.1.4 Boundary EC7

Boundary EC7 is a local boundary that encompasses the north east of England, predominately a 275kV ring serving local demand but crossed by one of the two of the 400kV North-South export routes from Scotland. This area is constrained by north-south power flows with the 400kV circuits at the southern end of the boundary. This boundary is

already at its limit for further generation and would require onshore reinforcement to facilitate additional generation.

3.2 Wider System Boundaries

3.2.1 Boundary B7

Boundary B7 bisects England south of Teesside. It is characterised by three 400kV double circuits, two in the east and one in the west. The area between B6 and B7 is traditionally an exporting area, and constrained by the power flowing through the region from Scotland towards the South with the generation surplus from this area added. In 2021, the required transfer exceeds boundary capability by about 600MW, increasing to about 2.3GW by 2030. This represents the level reinforcement required for compliance across B7 (see Figure 2).

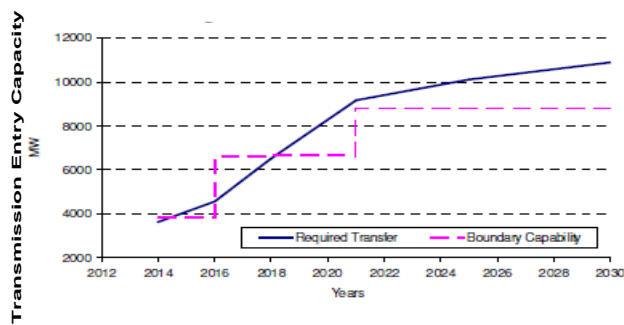


Figure 2. Reinforcement requirement B7

3.2.2 Boundary B7a

Boundary B7a runs parallel with boundary B7, sharing the same path in the east, but encompassing Heysham, Hutton and Penwortham in the west. The region between Boundary B7 and B7a includes more generation than demand, further increasing the transfers from north to south. In 2021, the shortfall in boundary capability is about 600MW, rising to over 2.5GW by 2030 (see Figure 3).

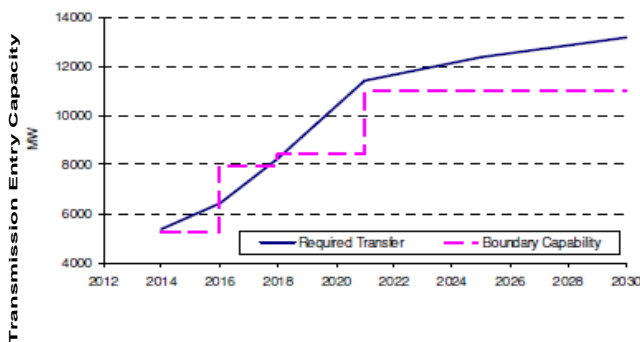


Figure 3. Reinforcement requirement B7a

3.2.3 Boundary B8

The North to Midlands boundary B8 is one of the wider boundaries that intersects the centre of Great Britain, separating the northern generation zones including Scotland, Northern England and Northern Wales from the Midlands and Southern demand centres. The east of B8 is traditionally a congested area due to the large amount of existing generation in the Humber and Aire valley regions. The current boundary capability is expected to drop between 2018 and 2021 due to changes in the generation background that reduce reactive capability. The shortfall in boundary capability in 2021 is about 3.5GW, rising to over 4.5GW by 2030 (see Figure 4).

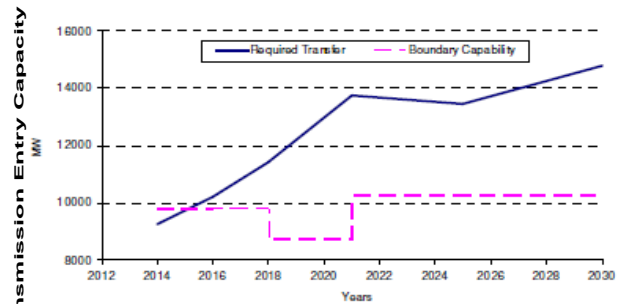


Figure 4. Reinforcement requirement B8

III. OFFSHORE INTEGRATED SOLUTIONS

From the results above it is clear that the connection of large scale offshore generation will require major network reinforcements either onshore or offshore for the wider system boundaries B7, B7a and B8. All the local system boundaries are close to their limit in capacity except Walpole area (Boundary EC3) which has spare capacity for up to 2GW before triggering further reinforcement. All these reinforcements will require extensive planning, consenting and construction programmes.

From past experience, National Grid would expect that planning and environmental issues for large scale onshore reinforcement activities would put delivery within the required timescales at significant risk. Therefore, a coordinated and integrated onshore and offshore development would lead to significant advantages to all parties.

Integrated offshore designs have been developed for two snapshot years; 2021, when the three large wind power plants may be reasonably considered as being 50% complete and 2030, when all wind farms are expected to be fully developed. The proposed designs employ a combination of:

- Offshore integration utilizes offshore AC interlinks within projects or HVDC links between offshore zones and onshore local boundaries, so as to provide boundary

capability, while minimising onshore works and optimizing asset sizes based on available technology.

- Onshore reinforcements include all possible works to provide capability onshore such as line upratings, re-conductoring, development of new onshore circuits and the use or installation of Quadrature Boosters.

The use of larger sized assets (e.g 2GW) has been assumed for projects connecting after 2019 so as to take advantage of anticipated advances in technology.

A. DESIGN FOR YEAR 2021

In 2021 the study results show a reinforcement requirement for B7 and B7a of about 600MW. Using the Economic Criterion, the wind scaling factor is assumed to be 70% and thus 1GW radial links to the shore will be utilised to only 700 MW. By installing AC links between the individual platforms within the Dogger Bank zone, the spare capacity on the two circuits that cross boundaries B7 and B7a (2 x 300MW) would provide the required boundary reinforcement.

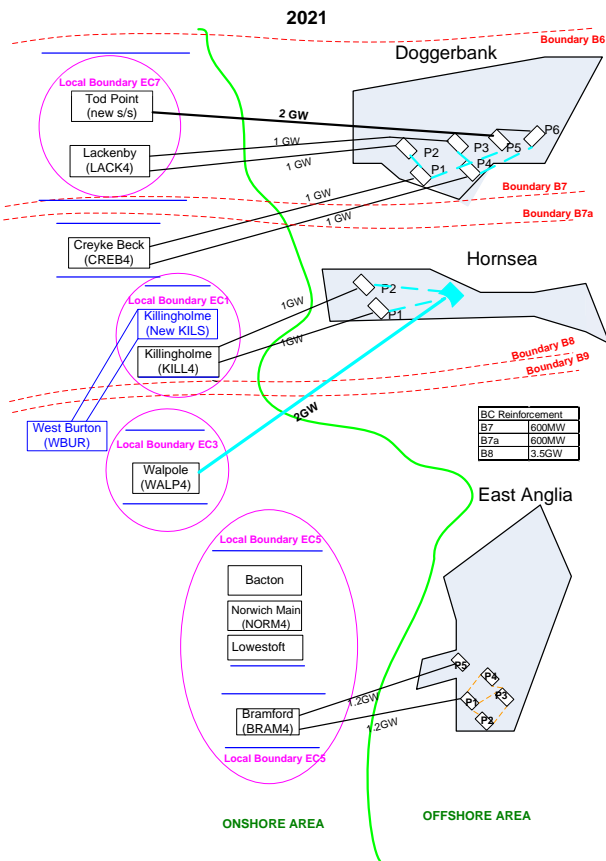


Figure 5. Offshore Integrated Design for 2021

In 2021, the reinforcement required across B8 is about 3.5GW. Offshore this could be achieved by integrating the two Hornsea platforms (P1, P2) with a new offshore platform which connects to Walpole via an HVDC link of 2GW capacity. The remaining 1.5GW capacity required across B8 can be achieved by an onshore reinforcement, Killingholme

South – West Burton. The combination of onshore and offshore reinforcement minimizes offshore cables and onshore converters, avoids onshore reinforcements at Walpole and facilitates the build-up of future connections by providing onshore capability in EC1. Figure 5 shows the proposed design alternative boundary reinforcements;

- Bootstrap Option: Two HVDC bootstraps between EC1 and EC3 with total capacity up to 3.5GW. These would not only trigger onshore reinforcements in both local boundaries but would also require multiple onshore converters.
- Onshore Option: To provide 3.5GW across B8 would require the Killingholme South – West Burton Upgrade, new circuits from Drax to Creyke Beck and Keadby as well as circuit re-conductoring.

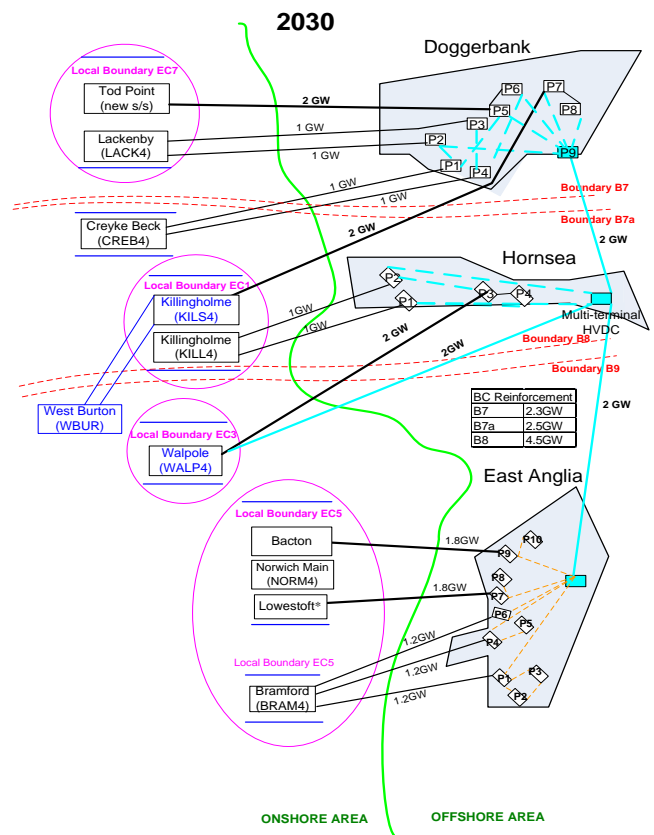


Figure 6. Offshore Integrated Design for 2030

B. DESIGN FOR YEAR 2030

By 2030 it is expected that the full capacity of Dogger Bank, Hornsea and East Anglia offshore wind farms will be connected to the system. At this time, B7 and B7a have a capacity shortfall of 2.3GW and 2.5GW respectively, while the B8 will require a reinforcement of about 4.5GW. The proposed design is presented in Figures 6.

This design provides a multi-terminal HVDC connection between Dogger Bank, Hornsea and East Anglia, and connects

onshore at Walpole. Offshore integration between all platforms within the Dogger Bank zone provides 1.5GW of boundary capability across B7 and B7a using the economic criteria as discussed earlier.

The platform for project P9 is oversized to 2GW to accommodate both the 1GW project (P9) and also provide an additional 1GW of boundary capability to help provide 2.5GW capability across B7 and B7a (1.5GW plus 1 GW oversize of asset). This 2GW platform connects to a platform in Hornsea via a 2GW HVDC link. Capability is provided across B8 via offshore links towards Walpole and East Anglia.

From the multi-terminal HVDC platform, one HVDC link rated at 2GW connects to Walpole. AC links connect to this platform from the Hornsea projects to provide capability across B8 and connect Dogger Bank P9 to Walpole. Integrating P3 and P4 provides an additional 600MW capability. Also, the Killingholme South – West Burton onshore reinforcement provides some capability across Boundary B8. Using the economy criteria described earlier, spare capacity within East Anglia region can be taken advantage of by providing an HVDC platform that integrates with AC links from the East Anglia projects. This provides 2GW boundary capability by connecting a 2GW HVDC link from the multi-terminal HVDC to the platform in East Anglia. This provides a total capability of 4.5GW across B8.

This design requires onshore reinforcements at Walpole EC3 to accommodate the additional 2GW. Dogger Bank Projects 7 and 8 take advantage of the capability provided at Killingholme South.

Alternative boundary reinforcements;

- Bootstrap option: Two HVDC bootstrap links would be required as shown in Figure 7, one between EC7 and EC3 zone to provide 2.5GW across B7, B7a and B8. A second 2GW link would be required between EC1 and EC5 to bring the total capability to 4.5GW. However, significant onshore constraints of both capacity and space would limit connections to boundaries EC7, EC3 and EC1, also, technology limitations could increase the number of cables required.
- Onshore Option: To provide 2.5 GW across B7, and B7a requires a new AC Circuit from Norton-Padiham (over 100km), re-conductoring Lackenby-Norton and Pewortham South circuits as well as completing the Mersey ring upgrade. To provide 4.5GW across B8 requires the Killingholme South – West Burton Upgrade, new circuits from Drax to Creyke Beck and Keadby as well as circuit re-conductoring. Also, Unified Power Flow Controllers (UPFC) would also be required at four substations to control power flows and voltage in the region.

The proposed integrated design will minimize onshore reinforcements and converter footprint onshore. It will increase the utilisation of the existing assets, by taking advantage of the spare capability within Dogger Bank, Hornsea and East Anglia zones.

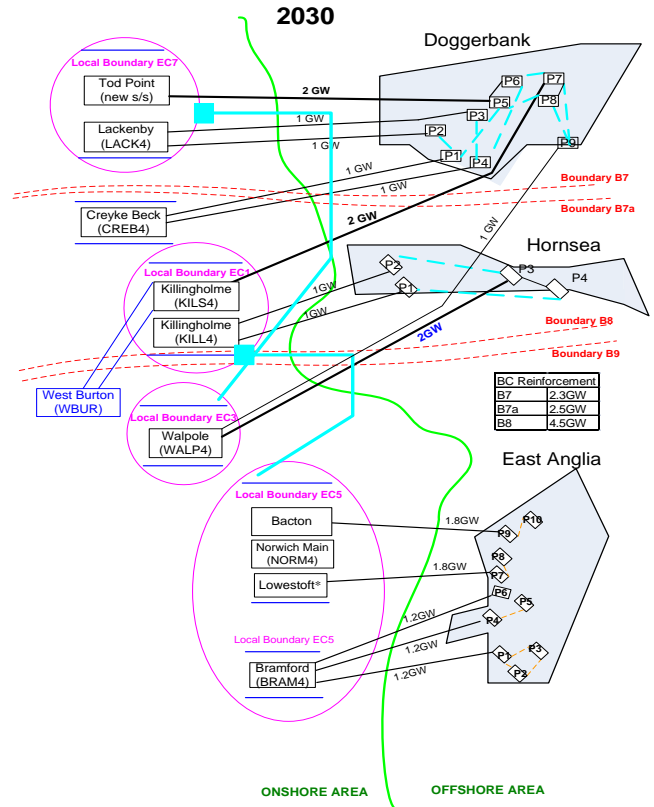


Figure 7. Coastal interconnection design for 2030

IV. CONCLUSION

The growth of offshore wind will raise several challenges in planning and operation of the GB transmission system. Integrating the offshore wind power plant networks and co-ordinating with onshore transmission works will decrease the environmental impact, improve the utilisation of assets and minimise wind power constraints.

The designs presented in this paper demonstrated the benefits of interconnecting offshore wind power plants to enhance wider system boundary capabilities. The connection of large offshore wind power plants at Dogger Bank, Hornsea and East Anglia both drive the need for reinforcement of system boundaries B7, B7a and B8 and offer, through offshore interconnection of their individual offshore networks, the solution.

The offshore interconnection adds North-South boundary capability to multiple boundaries from the North-East, through the Humber region and further South to East Anglia as well as relieving the local boundaries around the direct connection points onshore. During fault conditions it becomes possible to

reduce the power injection into stressed areas from the offshore wind power plants without constraining the offshore wind generation, assuming it is not operating at 100% output at this time. The benefits of onshore transmission development with interconnection of individual offshore networks

demonstrate the need for inclusion of offshore interconnection into existing NETS SQSS Chapter 4. While the case for integrating onshore and offshore transmission design have been demonstrated in this paper the financial framework to incentivise commercial wind power plant developers to include these offshore interconnections in their projects has yet to be worked out.

REFERENCES

- [1] Electricity Ten Year Statement, 2012, National Grid, www.nationalgrid.com
- [2] National Electricity Transmission System Security and Quality of Supply Standard, *National Grid*, www.nationalgrid.com
- [3] <http://www2.nationalgrid.com/UK/Services/Electricity-connections/Industry-products/TEC-Register/>



A new configuration of vertical axis wind turbine: an overview on efficiency and dynamic behaviour

垂直轴风力涡轮机的一种新配置： 对其效率与动态行为之概览

Mario R. Chiarelli¹, Andrea Massai², Davide Atzeni^{1*} and Francesco Bianco¹

¹Department of Civil and Industrial Engineering, University of Pisa, Pisa, Italy

²AM Engineering, Firenze, Italy

atzeni.dav@gmail.com

Accepted for publication on 3rd January 2015

Abstract - Preliminary results obtained for a new configuration “lift based” vertical axis wind turbine is shown. The turbine rotor is a cross flow fan type characterized by a high solidity and having the blades made of high curvature aerodynamic profiles which allow it to start at very low wind speed. A reduced scale model (Rotor diameter = 250mm, rotor height = 210mm , 24 blades) has been tested at the Department of Aerospace Engineering of Pisa showing an efficiency of about 18%.

During the test, a complete analysis of its aeroelastic response has been carried out using four strain gauges properly placed. Good correlation with FSI and rotor dynamic analyses have been obtained. Furthermore, steady and unsteady CFD simulations have been carried out using Ansys Fluent® Rel.14 and STAR-CCM+® Rel. 6.04 with the Moving Reference Frame and Moving Mesh techniques. CFD analyses confirm the results and give important information about its behaviour and the aerodynamic loads to which it is subjected. Noticeable scale effects have been found numerically, so, the efficiency of a full-scale lift based vertical axis optimized wind turbine is expected to be comparable with lift based horizontal axis wind turbine, i.e. around 30%.

A full-scale model of diameter = 1m and height = 1m, not discussed in this work, is currently under construction and will be tested in field to validate the numerical results. An efficiency of about 22% is expected. Since its optimal angular velocity decreases as the scale increases, vibrational phenomena for the full-scale model are supposed to be almost null. Due to its simplicity and its principle of operation, hydrodynamics applications are also quite promising

Keywords – Wind energy, Vertical axis wind turbine, VAWT, CFD.

I. INTRODUCTION

At the Department of Aerospace Engineering of the University of Pisa a research activity has been carried out concerning the development of a high efficiency vertical axis wind turbine in order to demonstrate the feasibility of a diffuse and competitive (low cost) electrical energy system generation.

Recently new configurations of these machines assume, more and more, the shape of a cross flow fan. These vertical axis wind turbine configurations, studied also by the authors of the present paper, start substantially from an early idea of machine: the *Lafond turbine*, shown in Champly [1], that, from a practical point of view, can be classified as a cross flow fan without the casing.

As it is well known in literature, the efficiency of traditional vertical axis machines are lower than the efficiency of horizontal axis machines. The difference of the turbine studied in this paper consists on the aerodynamic shape of its blades, Fig.1. Promoting several studies (i.e. Di Filippo [2], Russo [3], Atzeni [4] and Bianco [6]), the authors of the present paper observed that two dimensional CFD analyses, carried out on a Lafond turbine with $D = 10\text{m}$ having 24 blades, provided high values of the aerodynamic efficiency of the rotor. Starting from the layout examined by Russo [3], a carbon fiber prototype has been manufactured and tested in the wind tunnel available at the Department of Aerospace Engineering of Pisa (DIA), Fig.2.

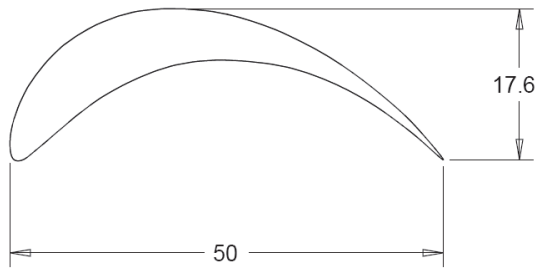


Fig. 1, Blade section. Units: mm. From Russo [3]

measured especially for high values of angular velocity, as shown in Fig.6 for the case at V=15m/s, being

$$\lambda = \frac{\omega R}{V} \tag{1}$$

$$\eta = \frac{\text{Turbine power}}{\text{Wind power}} = \frac{\omega M_z}{\frac{1}{2} \rho S V^3} \tag{2}$$

In any case, the efficiency measured at DIA agrees with some results available in literature concerning small scale rotor models. For example in the work of Colley [7], two dimensional simulations for a rotor with a diameter of 1.4m provide maximum efficiency between 15% and 25%. Have to be taken into account that these results have been obtained using stator-rotor configuration.

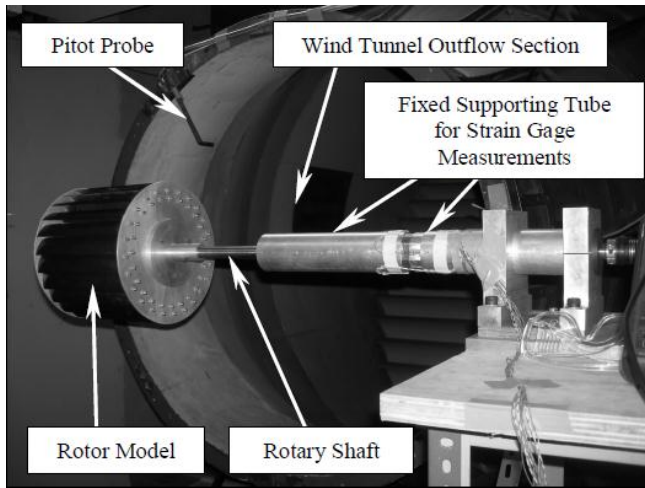


Fig. 2, Sketch of the wind tunnel test arrangement at DIA

Test results have shown that the maximum values of reduced scale rotor efficiency is about 18%, on the other hands, during tests non-negligible vibration effects have been observed.

II. CFD RESULTS

The ANSYS Fluent® CFD software has been used. The numerical values of torque have been obtained using a first level grid refinement, Fig.5. Numerical results have been obtained using Moving Reference Frame (MRF) technique, applied to a small area surrounding the blades, and K-ε turbulence model in steady state simulations. Results are in good agreement with experimental measurements.

CFD simulation also allowed to visualize flow path lines, shown in Fig. 3, in order to validate the general behaviour of the turbine. As reference has been taken the work from Gabi et al. [8], Fig.4. Nevertheless refining the grid and performing both steady and unsteady analyses applying MRF and Moving Mesh (MM) techniques, higher values of efficiency have been found. From a numerical point of view using a refined is possible to better describe the pressure field on each blade (boundary layer refinement has been also applied), while from a physical point of view, the vibration effects observed during the tests have, probably, reduced the values of torque

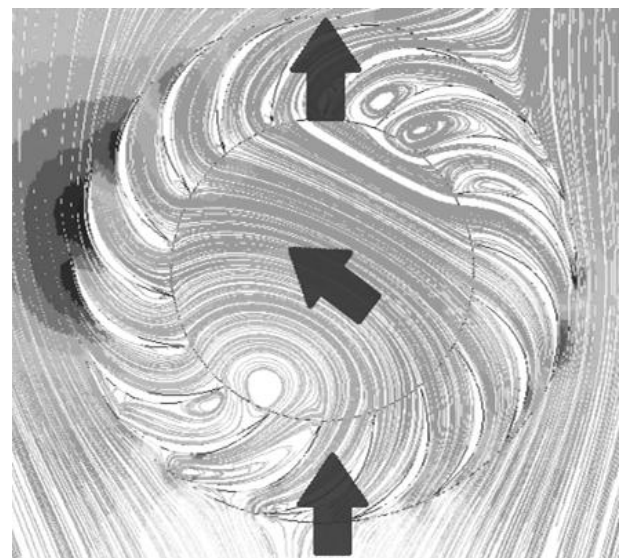


Fig. 3, Path lines - 2D CFD analysis from Russo [3]

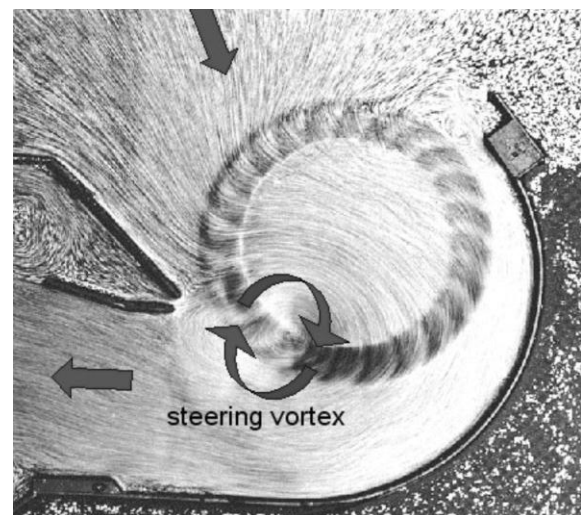


Fig. 4, View of fluid flow for a cross-flow fan in Gabi et al. [8]

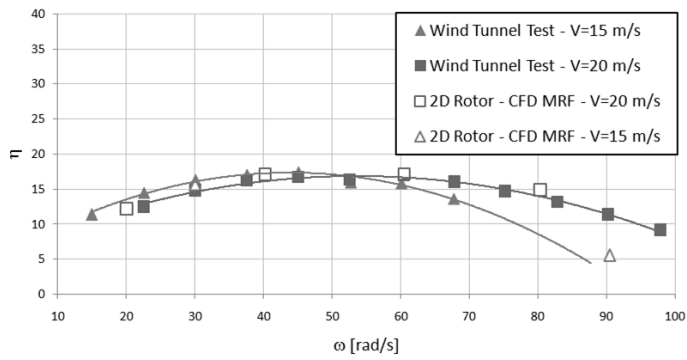


Fig. 5, Measured efficiency vs. 2D CFD MRF steady state analyses.

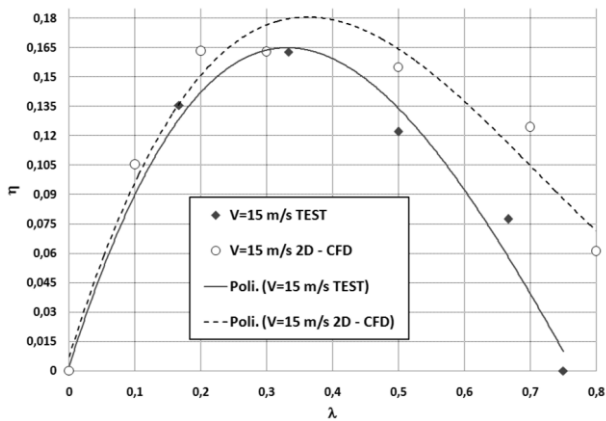


Fig. 6, Efficiency η vs. Tip Speed Ratio λ - case $V = 15$ m/s

In order to better understand the physics driving the turbine behaviour, polar plots of the contribute of any single blade have been drawn. In Fig. 7, Fig. 8 and Fig.9 those graph are reported for the case $V = 15$ m/s, flow coming from 180° . In this way is possible to see which blade is generating torque and which is opposing to the motion. Due to the high solidity coefficient, defined as:

$$\sigma = n \frac{c}{D} \tag{3}$$

These plots also describe the average load on a single blade during a complete rotation. Aerodynamics coefficients for the rotor prototype described above are calculated as:

$$C_{x,y} = \frac{F_{x,y}}{\frac{1}{2} \rho S V^2} \tag{4}$$

$$C_m = \frac{M_z}{\frac{1}{2} \rho S V^2 h} \tag{5}$$

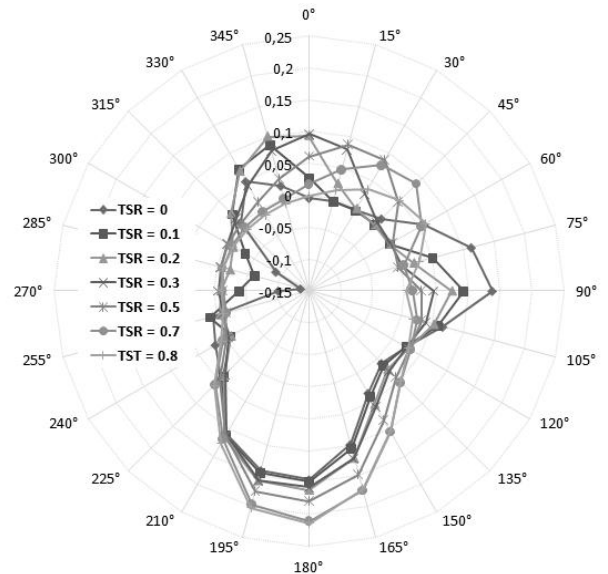


Fig. 7, C_y for the case $V = 15$ m/s - 2D CFD

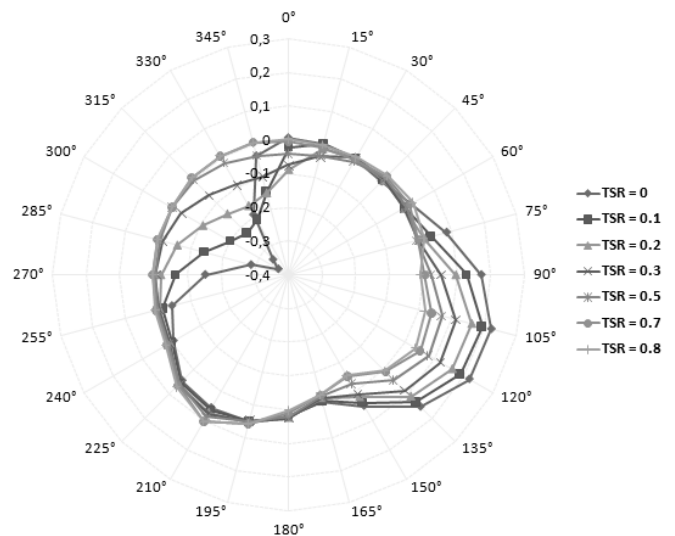


Fig. 8, C_x for the case $V = 15$ m/s - 2D CFD

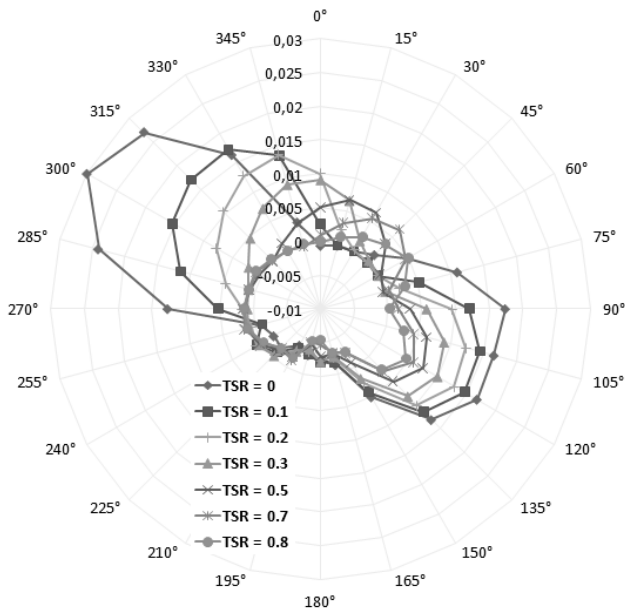


Fig. 9, C_m for the case $V = 15 \text{ m/s}$ – 2D CFD

The total values of these coefficients is reported for the case $V = 15 \text{ m/s}$ in Fig. 10. As can be seen the total C_y coefficient, namely the in-line load, tends to approach a constant value as the TSR value increase, while the C_x coefficient, namely the cross-flow load, change direction during the motion. It is important to underline that the C_x value is very low in the range of maximum efficiency.

No information are available at the moment on the value of axial forces and on the torque coefficient with respect to the other axes

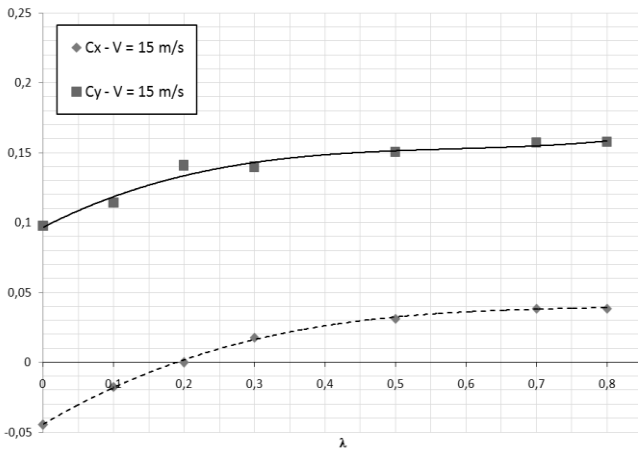


Fig. 10, Load coefficients for the case $V = 15 \text{ m/s}$ – 2D CFD

II. VIBRATIONAL ANALYSIS

As has already been mentioned, vibrational phenomena have been observed during the test. Load measurements were taken installing four strain gauges on the fixed support surrounding the rotor shaft, as described in Bianco [6] and Atzeni [5].

Load measurements were affected by inertial forces and, for this reason, no comparison between test and simulation is available. By the way sampling the strain gauges output signal and applying to it an FFT analysis, It has been possible to measure the complete rotor dynamical behaviour of the prototype. Waterfall plot have been drawn as shown in Fig. 11 and Fig.12, respectively the in-line F_y load and the cross-flow F_x load.

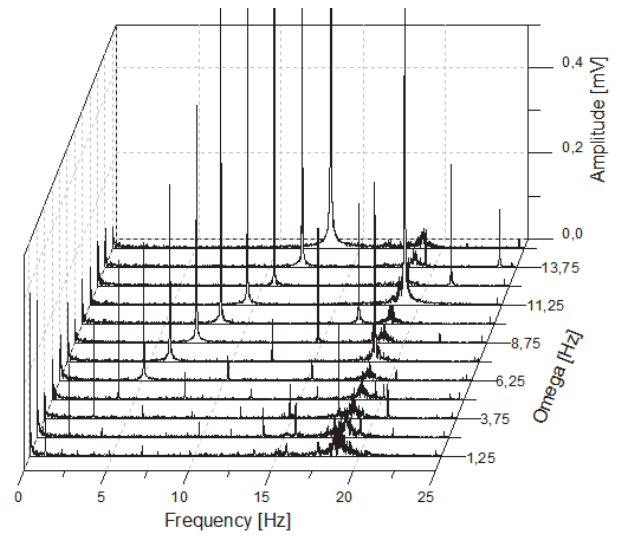


Fig. 11, F_y waterfall plot – Test

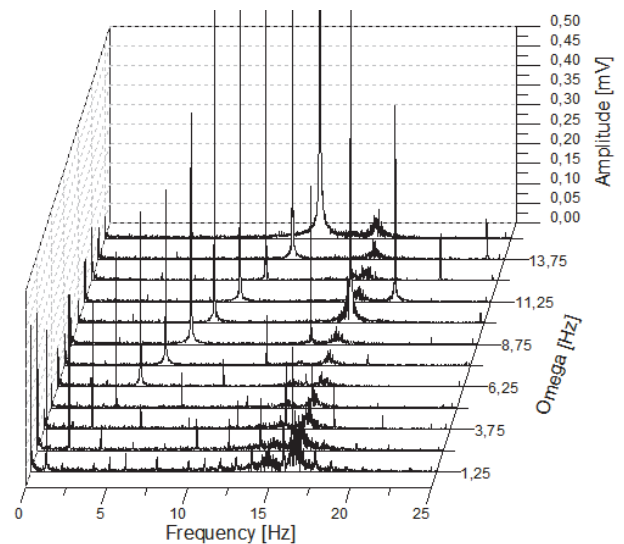


Fig. 12, F_x waterfall plot – Test

According to literature, for example Nelson [9] and Genta [10], combined effects of rotor dynamic natural response mode and first flexional response mode are clearly visible. Response amplitude is amplified in the range of angular velocity between 8 Hz – 15 Hz, namely for TSR between 0.42 – 0.8, exactly in the range of efficiency loss previously shown in Fig.6. Synchronous whirl and second whirl are clearly detectable. The slight difference between first natural mode in Y (about 18 Hz) and X (about 15 Hz) direction is due to a non complete symmetry of the system. Unfortunately no data are available on rotational dynamics since the first torsional mode was much above the sensitivity of the sensors. By the way unsteady two dimensional CFD simulation showed a frequency content in vortex detachment above 200 Hz.

Is important to underline that whirling phenomena are typical, and almost exclusive, of high rotating speed systems . Due to small displacements it is licit to assume that these phenomena do not affect the 2D assumption used in most of the simulations.

In normal case of wind energy harvesting, hence for dimensional scale of about 3m – 10m, maximum rotational speed for TSR = 0.9 would be between 9 rad/s – 2.7 rad/s at V = 15 m/s. In Bianco [6] and Atzeni [5] is shown that efficiency increase with Reynolds number. For this reason a noticeable scale effect is expected, as shown in Fig.13.

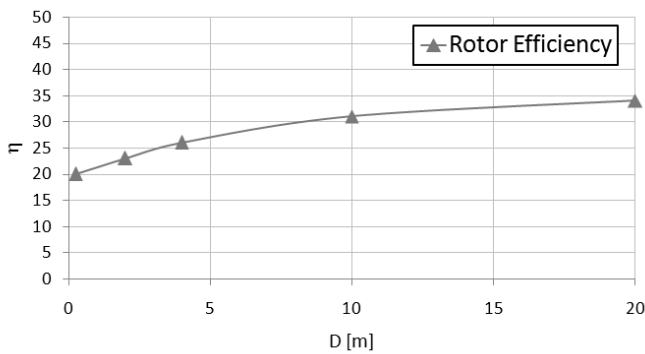


Fig. 13, Efficiency vs rotor scale

III. CONCLUSIONS

Results from a preliminary campaign tests carried out at the DIA of Pisa on a small scale rotor model have been shown. At the same time a campaign of two dimensional numerical analyses has been executed to estimate the behaviour of the rotor model both in small scale and real scale dimensions. Even if the experimental tests have been affected by unwanted vibration phenomena numerical and experimental results are in a good agreement.

The comparison has been carried out using the Fluent® code (Moving Reference Frame method of analysis applied only to the grid around the blades) with a first level refinement grid. The maximum value of the estimated efficiency is equal to 18%. Refining the mesh It has been possible to detect real behaviour in absence of vibrational phenomena. Dynamic behaviour of the rotor have been also studied in order to

validate initial assumption. By the means of CFD simulation a noticeable scale effect has been described. Currently a bigger prototype of 1m of diameter is under development. Because of its simplicity this turbine is also suitable for marine applications.

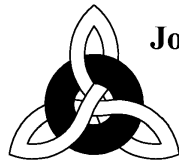
NOMENCLATURE

λ	Tip Speed Ratio (TSR)
ω	Rotational velocity
R	External rotor radius
V	Wind speed
σ	Rotor solidity
n	Number of blades
c	Chord of blade section
D	External rotor diameter
F	Aerodynamic load
M	Aerodynamic torque
C	Aerodynamic coefficient
ρ	Air density
S	Frontal surface ($D * h$)
h	Rotor height
η	Rotor efficiency
MRF	Moving Reference Frame technique
MM	Moving Mesh technique
DIA	Department of Aerospace Engineering (Pisa, Italy)

REFERENCES

- [1] R. Champly. “Les moteurs a vent: théorie, construction, montage, utilisation au puisage de l’eau et à la production de l’électricité”, Dunod, Paris, 1933
- [2] A. Di Filippo. “ A two dimensional numerical simulation to calculate and to optimise the efficiency of a vertical axis wind turbine”, *First level degree thesis*, Department of Aerospace Engineering, CD-ROM n 193 2005/2006, University of Pisa, 2007.
- [3] G. Russo. “Three dimensional modelling and preliminary fluid dynamics study of a vertical axis wind turbine prototype”, *First level degree thesis*, Department of Aerospace Engineering, CD-ROM n. 281 2006/2007, University of Pisa, 2008.
- [4] D. Atzeni. “Estimation of the aerodynamic efficiency of a vertical axis wind turbine by means of two dimensional and three dimensional CFD simulations”, *First level degree thesis*, Department of Aerospace Engineering, CD-ROM n. 300 2006/2007, University of Pisa, 2008.
- [5] D. Atzeni. “A numerical study and preliminary experimental analysis of the dynamic of a vertical axis micro wind turbine”, *Master level degree thesis*, Department of Aerospace Engineering, Web Ref: <http://etd.adm.unipi.it/theses/available/etd-05012012-101812/>, University of Pisa, 2012.
- [6] F. Bianco, “Experimental study, validation of the three dimensional CFD model and scale effect prediction of a vertical axis wind turbine”, *First level degree thesis*, Department of Aerospace Engineering, Web. Ref:

- <http://etd.adm.unipi.it/theses/available/etd-03212014-194526/>, University of Pisa, 2013.
- [7] G.Colley, R.Mishra, H.V. Rao, R.Woolhead, "Effect of rotor blade position on vertical axis wind turbine performance", *International Conference on Renewable Energies and Power Quality (ICREPQ'10)*, Granada, Spain, 2010.
- [8] M. Gabi, T. Klemm, "Numerical and experimental investigation of cross-flow fans", *Journal of computation and applied mechanics*, Miskolc University Press, **5(2)**, 251-261, 2004.
- [9] F.C.Nelson, "Rotor dynamics without equations", *International Journal of COMADEM*, **10 (3)**, 2 – 10, 2007.
- [10] G.Genta, "Dynamics of rotating systems", *Mechanical engineering series*, Spinger press, Italy, 2005
- [11] M.Chiarelli, A.Massai, D.Atzeni, F.Bianco, "A New Configuration of Vertical Axis Wind Turbine for a Distributed and Efficient Wind Power Generation System", *Wind Engineering*, **37 (3)**, 305-320, Multi science publishing, UK, 2013.



**Journal of Energy Challenges
and Mechanics**

ISSN 2056-9386

<http://www.nscj.co.uk/JECM/>

Editor:

Dr. Henry Tan
University of Aberdeen, Scotland, United Kingdom

Scope:

Since James Watt, a Scottish inventor, improved efficiency of the steam engine, human civilization relies more and more on a steady supply of energy. Today we are at a transitional age. On the one hand, we see technology advances in the exploration and development of oil and gas, a depleting resource; we see growth in handling aging and decommissioning. On the other hand, we see ideas and plans for new energy infrastructure. This journal is about energy challenges and the underlying mechanics, involving multiple disciplines in science, technology, management and policy-making. Mechanics, fundamentally, is about force and the related behaviours, where force is about relationships, including those physical, human and social. For mechanics, the journal covers interactive boundaries with many other disciplines. For energy, topics include both fossil fuels and many different forms of renewable energy; also, issues related to energy economy, energy policy, efficiency, safety, environment and ecology will also be covered.



Cove Bay, Aberdeen, Scotland, United Kingdom